

EFFECT OF EXPERIMENTAL PARAMETERS ON SIMULTANEOUS THERMAL  
ANALYSIS

Except where reference is made to the work of others, the work described in this thesis is my own or was done in collaboration with my advisory committee.  
This thesis does not include proprietary or classified information.

---

Rui Shao

Certificate of Approval:

---

Jeffrey W. Fergus  
Associate Professor  
Materials Engineering

---

Ruel A. Overfelt, Chair  
Professor  
Materials Engineering

---

Aleksandr Ludvigovich Simonian  
Professor  
Materials Engineering

---

George T. Flower  
Interim Dean  
Graduate School

EFFECT OF EXPERIMENTAL PARAMETERS ON SIMULTANEOUS THERMAL  
ANALYSIS

Rui Shao

A Thesis

Submitted to

the Graduate Faculty of

Auburn University

in Partial Fulfillment of the

Requirements for the

Degree of

Master of Science

Auburn, Alabama  
May 10, 2007

EFFECT OF EXPERIMENTAL PARAMETERS ON SIMULTANEOUS THERMAL  
ANALYSIS

Rui Shao

Permission is granted to Auburn University to make copies of this thesis at its discretion,  
upon request of individuals or institutions and at their expense.  
The author reserves all publication rights.

---

Signature of Author

---

Date of Graduation

## VITA

Rui Shao, daughter of JinDe Shao and LianFang Li, was born on December 15, 1970 in He Nan, P. R. China. She attended Northeastern University, Shenyang, China from September 1988 to July 1992, and received a degree of Bachelor of Science in the Department of Nonferrous Metallurgy Engineering in 1992. She continued her graduate study immediately after graduation, entering the Department of Materials Science and Engineering at the same university. After she obtained the Master of Science in 1995, she moved to Singapore and worked in several chemical companies as a chemical engineer and chemist. In 1997 Rui joined to the Department of Materials Science and Engineering as a Technical Officer at Nanyang Technology University, where she worked for more than 5 years. After moving to the U.S., she enrolled in the graduate study program in Materials Engineering at Auburn University in 2003. She married Cai Liang on February 8, 1995. Rui and Cai are blessed with a daughter, Susanna, and a son, William.

## THESIS ABSTRACT

# EFFECT OF EXPERIMENTAL PARAMETERS ON SIMULTANEOUS THERMAL ANALYSIS

Rui Shao

Master of Science, May 10, 2007  
(B.S., Northeastern University, Shenyang, P. R. China, 1992  
M.S., Northeastern University, Shenyang, P. R. China, 1995)

95 Typed Pages

Directed by Ruel A. Overfelt

Differential Scanning Calorimeter (DSC) is a very effective way to measure both the heat capacity and the phase transition temperature in thermal processes. With the continued development of computational models of thermal processes, the accuracy of the thermophysical data plays an increasingly key role in the final simulation results. However, since DSC is a transient measurement process and a relative technique, the experimental parameters must be carefully considered. This study combined DSC with

Thermogravimetric Analysis (TGA) to examine the influence of the various interrelated measurement parameters.

This thesis consists of two sections: First, the experimental parameters of the heating rate and specimen characteristics (mass and geometry) and their effects on measurements of the transition temperature and enthalpy are considered and appropriate calibration factors determined. This is followed by an examination of the effect of oxidation on the measurements.

In the first part of this work, the effects of several factors on the phase transition temperature and the transition enthalpy were examined, separately. To determine the effect of experimental parameters on the phase transition temperature, a deviation method is proposed to determine the initial phase transition temperature rather than the onset temperature as is typically used in the literature. Next, a study of the effect of sample geometry indicated that the measured phase transition temperature is reduced with decreasing particle size, but the effect from the sample mass is not significant. The phase transition enthalpy decreased with both the heating rate and the total surface area of the sample, suggesting that the oxidation of samples in the measuring process should be taken into account.

The second section of this research focused on analyzing the effect of oxidation on specific heat capacity ( $C_p$ ) measurements. The contribution of sample oxidation to the deviation of the heat capacity measurement could be classified in term of two factors: one being the amount of oxide generated and the other the heat released by the oxidation reaction. The results revealed that the influence of the heat capacity from the reaction enthalpy was more significant than that from the generated oxide.

## ACKNOWLEDGMENTS

I would like to express my grateful appreciation to Dr. Ruel A. Overfelt for his guidance and his constant encouragement in pursuit of this degree. He is an inspiring professor and an excellent mentor. His example has taught me how to be an ethical researcher. Without his enormous patience and endurance, I would not have accomplished my objectives.

I also want to extend my thanks to my other committee members, Dr. Jeff Fergus and Dr. Simonian, for their valuable suggestions and help in the course of this study.

My gratitude also goes to Dr. Rick Williams, for his friendship and constant support both before and after he left Auburn University. I really enjoyed working under his supervision.

Thanks are due to my group members: Bao Jian Guo and George Teodorescu, for their friendship and help throughout.

Finally, I am most grateful to my husband for his collaboration as we worked together to care for our children as well as to my parents for their love, support and understanding.

Style manual or journal used: Auburn University Manual and Guide for the Preparation  
of Theses and Dissertations

Computer software used: Microsoft Office 2003, Matlab7.0



## TABLE OF CONTENTS

LIST OF TABLES.....	xii
LIST OF FIGURES.....	xiii
1. INTRODUCTION .....	1
2. LITERATURE REVIEW .....	6
2.1. Current research on the phase transition temperature and enthalpy measurements by DSC .....	6
2.2. Methods to calibrate the phase transition temperature and enthalpy .....	10
2.3. Effect of oxidation on specific heat capacity measurements .....	14
3. EXPERIMENTAL PROCEDURE AND ANALYTICAL TECHNIQUES.....	15
3.1. Simultaneous Thermal Analysis 1500 (STA1500) instrument .....	15
3.2. Experimental set-up to determine the effects on phase transition temperature and enthalpy measurement .....	17
3.2.1. Determination of phase transition temperature .....	17
3.2.2. Experimental set-up to determine the effects of experimental variables .. .....	20
3.2.3. Experimental set-up for sensitivity calibration .....	24
3.2.4. Calculation of the heat calibration factor .....	25
3.3. Effect of oxidation on specific heat capacity ( $C_p$ ) measurements.....	26
3.3.1. Experimental set-up for $C_p$ measurement.....	26

3.3.2.	Method for calculating $C_p$ from DSC results .....	27
3.3.3.	Calculation of the generated oxide effect on $C_p$ measurement .....	29
3.3.4.	Calculation of the effect of oxidation reaction enthalpy on $C_p$ measurement.....	30
4.	RESULTS AND DISCUSSION .....	33
4.1.	Melting point temperature measurements .....	33
4.1.1.	Analysis of raw experimental results .....	33
4.1.2.	Effect of heating rate on the phase transition temperature.....	37
4.1.3.	Effect of sample mass on phase transition temperature .....	42
4.1.4.	Effect of sample geometry on phase transition temperature .....	47
4.2.	Transition heat measurements .....	51
4.2.1.	Sensitivity calibration.....	51
4.2.2.	Phase transition enthalpy measurements.....	54
4.2.2.1.	Effect of heating rate on phase transition heat measurements	57
4.2.2.2.	Effect of sample mass and geometry on phase transition enthalpy measurements.....	59
4.2.2.3.	Relationship between heat calibration factor and total surface area.....	61
4.3.	Calculation of the oxidation effect on $C_p$ measurement.....	62
4.3.1.	The effect of the presence of aluminum oxide on $C_p$ measurements ....	62
4.3.2.	Effect of the oxidation reaction enthalpy on $C_p$ measurements .....	66

5. CONCLUSIONS.....	72
6. SUGGESTIONS FOR FUTURE RESEARCH.....	73
REFERENCES.....	74

## LIST OF TABLES

Table 1-1	Summary of thermal analysis techniques .....	2
Table 3-1	Experimental design to examine the effect of heating rate on the phase transition temperature .....	21
Table 3-2	Particle size distributions of aluminum powder samples.....	23
Table 3-3	Experimental designs to examine the effect of sample mass.....	24
Table 3-4	Coefficients of the reaction enthalpy (NIST, 2005).....	32
Table 4-1	Phase transition temperatures of zinc and aluminum .....	37
Table 4-2	Temperature correction factors.....	40
Table 4-3	Initial transition temperature for samples with different masses under heating rates of 10 °C/min and 20 °C/min.....	44
Table 4-4	Initial transition temperature for various mean particle sizes.....	49
Table 4-5	Measured transition heat of aluminum under each measuring condition .	56
Table 4-6	Calculation results for the oxidation reaction heat flow .....	67

## LIST OF FIGURES

Figure 1-1	Typical Simultaneous Thermal Analysis (STA1500) data (aluminum pellet 20mg, 20°C/min).....	3
Figure 1-2	Interpretation of STA1500 results .....	4
Figure 2-1	Ideal sample signal and real measured signal in the case of a first order transition in the sample: .....	8
Figure 2-2	Definition of characteristic temperatures of a peak (Höhne et al., 1990). 11	
Figure 2-3	Results of the eutectic temperature of Co-18.5 at %Al after initial calibration and correction (Wu and Perepezko, 2000).....	12
Figure 2-4	Enthalpy calibration factor plotted against transition temperature for gallium, indium and tin. (Gmelin and Sarge, 1995) .....	13
Figure 3-1	(a) Simultaneous Thermal Analyzer1500 (Rheometric Scientific, Inc.), (b) schematic drawing of the main module and the hang-down. ....	16
Figure 3-2	DSC trace for a typical melting peak per ASTM conventions .....	18
Figure 3-3	(a) Raw signal of STA in DSC mode, (b) First derivative of raw signal..	19
Figure 3-4	Particle size distribution of a) powder37, (b) powder112.....	22
Figure 3-5	Peak areas calculation of aluminum pellet samples.....	26
Figure 3-6	Heat capacity measurements using the conventional three-step method..	28
Figure 4-1	Raw data for aluminum pellet samples with varying heating rate as a function of (a) time, (b) temperature ( $T_m=660.1^\circ\text{C}$ ) .....	34

Figure 4-2	Raw data for zinc pellet samples with varying heating rate as a function of (a) time, (b) temperature ( $T_m=419.5^\circ\text{C}$ ).....	35
Figure 4-3	Initial phase transition temperature as a function of the heating rate .....	39
Figure 4-4	Temperature correction curve for pellet samples.....	41
Figure 4-5	Raw results for aluminum pellets with varying mass size at the indicated heating rates .....	43
Figure 4-6	Initial phase transition temperature of aluminum pellet samples as a function of mass size (uncorrected data) .....	45
Figure 4-7	Combination of the heating rate and mass effect on $T_i$ of aluminum pellet samples (uncorrected data) .....	46
Figure 4-8	Raw results of geometry effect on $T_i$ for aluminum samples with masses: 9.6mg, 20mg and 30mg .....	48
Figure 4-9	Effect of mass and particle size on $T_i$ of aluminum samples.....	50
Figure 4-10	Effect of aluminum particle size on the initial phase transition temperature .....	51
Figure 4-11	The net results for the standard sapphire disc at various heating rates.....	52
Figure 4-12	Sensitivity calibration at various heating rates .....	53
Figure 4-13	Effect of heating rate on heat calibration factor for aluminum pellet and powder.....	57
Figure 4-14	Effect of sample mass size and geometry on the heat calibration factor for various aluminum samples.....	60
Figure 4-15	Relationship of heat calibration factor and total surface area of aluminum . .....	61

Figure 4-16	The mass change of 20mg aluminum samples with various sample geometries.....	63
Figure 4-17	Aluminum oxide generated from aluminum with an initial sample mass of 20mg.....	64
Figure 4-18	Change in $C_p$ due to the presence of alumina surface film.....	65
Figure 4-19	Effects of oxidation reaction for 20mg aluminum: powder <sup>37</sup> and pellet.	68
Figure 4-20	Measured heat flow of standard sapphire and calculated true heat flow for aluminum.....	69
Figure 4-21	The corrected heat flow of aluminum powder and pellet samples by oxidation reaction enthalpy.....	70
Figure 4-22	Deviation in $C_p$ measurement due to the oxidation reaction.....	71

## 1. INTRODUCTION

As computing science continues to develop, more and more experiments are now carried out using computer simulations rather than actual experiments. The significant advantages of experiment simulation compared with traditional experiments include savings in materials, energy and labor. In order to obtain accurate simulation results, a good understanding of the physical properties of the materials is needed to construct the computational models. A material's thermal properties, including its specific heat capacity, phase transition temperature, thermal expansion coefficient and thermal diffusivity, play a key role in research on heat transfer phenomena (Wang et al., 2002; Fasoyinu et al., 2003).

Currently, most thermal property measurements are carried out using commercial devices (Hasegawa et al., 1980; Wendlandt, 1986; Speyer, 1994; Höhne et al., 2003). Table 1.1 lists the techniques typically used to determine thermal properties. Some techniques may be combined to form simultaneous thermal analysis techniques, for example STA, TG-FTIR, DSC-X-ray, etc.



Table 1-1 Summary of thermal analysis techniques

<b>Thermal property</b>	<b>Technique</b>	<b>Technique Acronym</b>
Mass	Thermogravimetric Analysis	TGA
	Evolved gas analysis	EGA
Phase transition temperature	Differential thermal analysis	DTA/DSC
Enthalpy	Differential scanning calorimetry	DSC
Dimensions	Thermodilatometry	-
Mechanical characteristics	Thermomechanical Analysis	TMA
	Dynamic Thermomechanical Analysis	DTMA

The most promising feature of the STA1500 equipment available in our lab for simultaneous thermal analysis from room temperature to 1500 °C is its ability to combine Thermogravimetric Analysis (TGA) with heat-flux type differential scanning calorimetry (DSC). Taking aluminum pellet as an example, a typical STA1500 measuring result in temperature scale is shown in Figure 1-1.

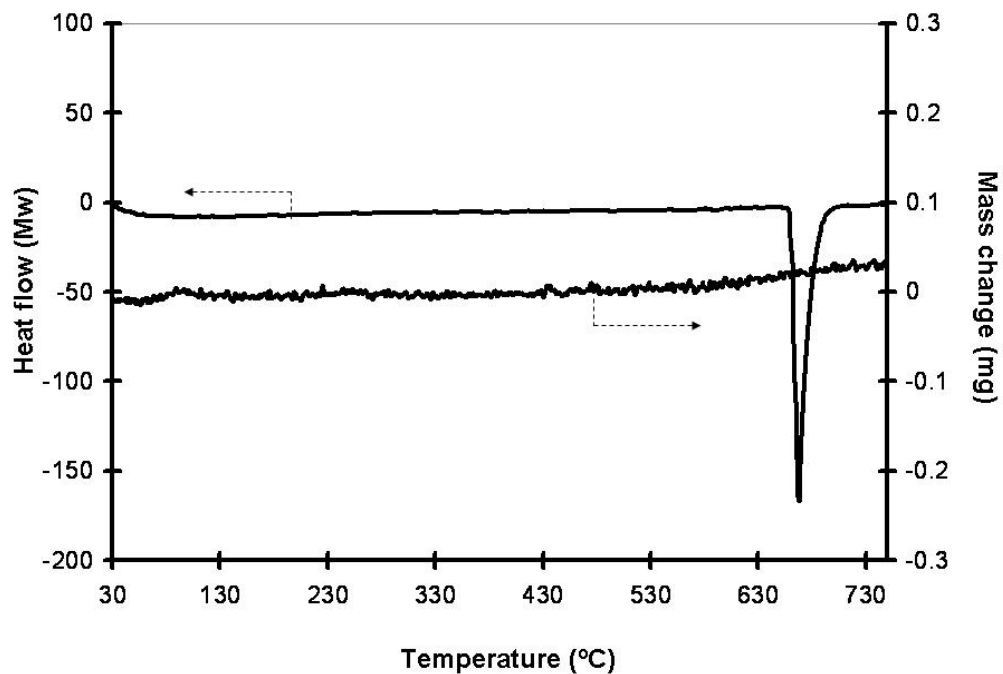


Figure 1-1 Typical Simultaneous Thermal Analysis (STA1500) data (aluminum pellet 20mg, 20°C/min)

DSC provides information showing how the heat flow varies with temperature or time, as well as the amount of heat absorbed or released during the thermal process (O'neil, 1966). Consequently, DSC can be used to study phenomena relevant to the thermal energy change such as the phase transition temperature, glass transition temperature, and melting point, as well as the heat change during the phase transition or chemical reaction, heat capacity measurements, and purity measurements. In contrast, typical TGA measurements provide information about changes in the sample mass during heating or cooling processes. Thus, combining DSC and TGA provides a powerful tool for interpreting thermal processes. Figure 1-2 shows typical combined DSC and TGA results for a number of common processes.

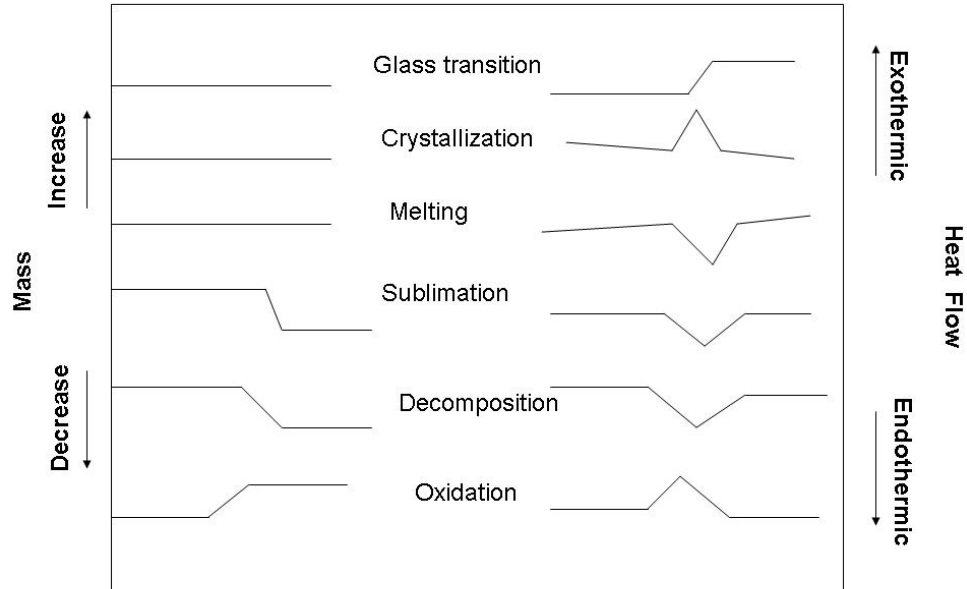


Figure 1-2 Interpretation of STA1500 results

The STA's features determine how the influence of the measuring parameters should be considered. Compared with other devices for measuring thermophysical properties, STA is a continuous, dynamic and relative technique. Therefore, the effects of different experimental parameters, (e.g., the heating rate, sample mass and geometry, as well as the operator-related factors) have been widely reported in the literature (Barrall, 1973; Wu and Perepezko, 2000; Ramakumar et al., 2001; Wolfinger et al., 2001; Nugene et al., 2003; Sarri et al., 2003; Jacob and Schlesinger, 2006).

Furthermore, effective correction methods have been proposed to improve the results. ASTM (American Society of Testing and Materials) procedures (e.g. ASTM-E967-97, 2000; ASTM-E968-99, 2000) are widely used in commercial DSC equipment to standardize the measurement results. GEFTA (German Society for Thermal Analysis) has also contributed extensively to this research effort (Höhne et al., 1990; Sarge et al., 1994; Gmelin and Sarge, 1995; Sarge et al., 1997; Gmelin and Sarge, 2000; Sarge et al., 2000). Compared with the ASTM method, GEFTA recommendations provide a more general temperature correction method that does not depend on the heating rate. Other specific methods can be found in Wu and Perepezko (2000) and Schawe (1993).

In this study to improve the accuracy obtainable using the STA1500, the research is divided into two sections. First, the effect of experimental parameters such as heating rate, sample mass and sample geometry (powder or pellet) on the melting temperature and phase transition heat was studied in DSC mode. In the second part of this work, the effect of oxidation on specific heat capacity ( $C_p$ ) measurements was studied using combined DSC and TGA. The results are expected to provide valuable information to facilitate the interpretation of results obtained using the STA1500.

## 2. LITERATURE REVIEW

DSC is a very effective technique for studying the phenomena involved in heat changes and it has been widely used in materials research since it was invented, for example in study of metal/alloys, ceramics and polymers (Wendlandt, 1986; Speyer, 1994) and the biological properties of proteins (Privalov and Potekhin, 1986; Sturtevant, 1987; Brandts and Lin, 1990; Freire et al., 1990). However, some researchers (Höhne 1983; Dong and Hunt, 2000; Ramakumar et al., 2001; Wolfinger et al., 2001; Nugene et al., 2003) have identified issues of possible misinterpretation of DSC results.

This literature review consists of three sections. The first section reviews current research trends in the measurement of phase transition temperature and transition heat using thermal analysis techniques. This is followed by a summary of some specific correction methods that are applied to obtain more accurate temperature and transition heat measurements, and the chapter concludes by examining and discussing the significance of potential sample oxidation during measurements.

### 2.1. Current research on the phase transition temperature and enthalpy measurements by DSC

The phase transition temperature between the solid and liquid phases can be determined by either the melting point ( $T_m$ ) during heating or the crystallization point ( $T_c$ ) during cooling. Theoretically,  $T_m$  should be equal to  $T_c$  (in the absence of supercooling)

but more factors are involved in the crystallization process than in the melting process. The phase transition from liquid to solid consists of crystal nucleation and growth processes, and some undercooling is required for nucleation. Consequently, the crystallization point is always lower than the equilibrium phase transition temperature. Moreover, a complex crystal structure magnifies the kinetic undercooling required, so researchers (Martins and Cruz-Pinto, 1999, Hakvoort et al., 2001) often rely upon calibration procedures for crystallization point measurement. In this study, only the melting process was characterized.

The melting point temperature is not a discrete point in continuous heating DSC; the phase transition of melting is expressed as a peak in DSC curves. For an ideal case, in which the total heat of fusion is input into the sample in an infinitely small time interval, the heat flux peak takes the form of a Dirac pulse (Figure 2-1 (a)); However, the phase transition peak measured by DSC is influenced by the experimental conditions. For example, a limited heat flux input into the sample due to the finite power supply available in real cases leads to a heat flow signal from the DSC that extends over a temperature range. Furthermore, the heat absorbed due to the sample melting results in a heat flow difference between the sample and the reference pan leading to an endothermic peak in the DSC measurement results. A linear heating rate produces a theoretical heat flow curve that exhibits a saw tooth triangle (Figure 2-1(b)). Additionally, in real measurements, experimental parameters such as the heating rate and the sample mass and geometry, as well as the thermal properties of the sample, sample pan and the standard sample, also influence the shape of the endothermic peak. This is known as “smear

effect” and arises due to the heat relaxation that occurs during the heating process. Consequently, the real endothermic peak for melting takes the shape illustrated in Figure 2-1(c).

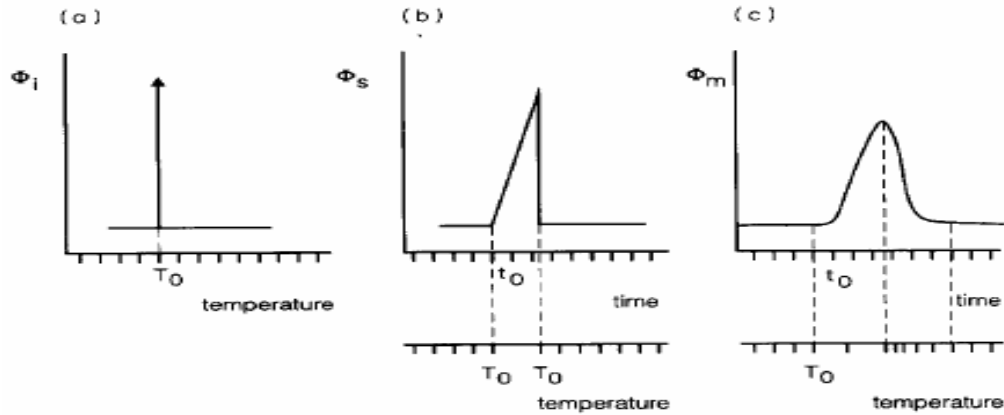


Figure 2-1 Ideal sample signal and real measured signal in the case of a first order transition in the sample:

(a) ideal infinite sample heat flow rate, (b) ideal but finite sample heat flow rate, (c) actual measured heat flow rate(Schawe, 1993).

Several factors cause this discrepancy between the measured results and the true values of the thermophysical properties. The most important are due to the features of DSC techniques and it is therefore necessary to identify methods to correct the measured results. First, the dynamic features of the DSC technique preclude achieving true equilibrium status (Callanan and Sullivan, 1986; Gmelin and Sarge, 1995). By definition, the melting point of a pure substance is the temperature where its solid and liquid phases are in equilibrium at atmospheric pressure. Second, indirect sample temperature measurement causes a deviation from the true phase transition temperature. The deviation

in the melting temperature in a heatflux type DSC has been studied theoretically. For example Dong and Hunt (2000) developed a numerical heat transfer model to describe the temperature difference between the heating plate (where the temperature sensor is located), and the sample. The temperature difference between the measured temperature (actually the heatflux plate temperature ( $T_p$ )) and the sample ( $T_s$ ) is caused by the heat transfer between the sample holder and sample, and the radiation heat lost from the sample holder and sample. The relationship between the sample temperature and the pan is:

$$T_p = T_s + \left( \frac{1}{H_{cp}} m_c c_c + \frac{1}{H_{sp}} m_s c_s \right) \frac{\Delta T}{\Delta t} - \frac{1}{H_{cp}} q_c - \frac{1}{H_{sp}} q_s \quad (2-1)$$

Where

$$\frac{1}{H_{sp}} = \frac{1}{H_{cp}} + \frac{1}{H_{sc}} \quad (2-2)$$

$H_{sp}$ ,  $H_{cp}$  and  $H_{sc}$  are the heat transfer coefficients from the crucible (sample pan) to the heating plate, from the crucible to the heating plate, and from the sample to the crucible, respectively.  $q_c$  and  $q_s$  are the radiation coefficients for the crucible and the sample, respectively.  $m_s$ ,  $m_c$  and  $c_c$ ,  $c_s$  are the masses and heat capacities of the sample and crucible, and  $\frac{\Delta T}{\Delta t}$  is the heating rate.

Other similar mathematical models can be found in Holubova et al. (2000) and Hakvoort et al. (2001).



The heat transfer feature of DSC means that the heating rate, the environment gas, and the properties of the specimen, such as its purity, geometry, and homogeneity, also play a part in the DSC measurement results. Höhne (1983) considered the non-linear heat transfer in DSC and calculated that the effect of experimental parameters such as the heating rate and sample mass on a heatflux type calorimeter was of the order of 1 to 5%.

## **2.2. Methods to calibrate the phase transition temperature and enthalpy**

Research (Mraw and Naas, 1979; Callanan et al., 1992; Skoglund and Fransson, 1996; Castro et al., 2000) indicates that the true thermophysical properties can be obtained using careful calibration. This literature review therefore summarizes the calibration methods most widely used in DSC measurement.

The ASTM standard (ASTM-E967-97, 2000) has been adopted by most commercial DSC instrument manufacturers. In this method, the temperature and transition heat are calibrated using two standard samples. The selection of standard samples is determined by the temperature range of interest; the desirable temperature point should fall between the melting points of the two standard samples. It is important to ensure that precisely the same measuring conditions are used for the standards and the unknown samples. If the experimental conditions (especially the heating rate) change, measurement on the standards must be repeated.

GEFTA, the German Society for Thermal Analysis, developed an alternative method for the phase transition temperature and transition heat calibration (Cammenga et al., 1993; Sarge et al., 1994; Sarge *et al.*, 1997; Gmelin and Sarge, 1995; Gmelin and Sarge, 2000; Gatta et al., 2006). For the temperature calibration, they took the onset temperature of the melting peak as the heating rate approached to zero  $T_{e(\beta \rightarrow 0)}$  as the true melting temperature ( $T_{true}$ ) (see Figure 2-2). The temperature correction curve was then constructed based on the onset temperature of two standard samples at a heating rate of zero. The true melting temperature of the specimen was then expressed as equation (2-3):

$$T_{true} = T_{e(\beta=0)} + \Delta T_{corr(\beta=0)} \quad (2-3)$$

where  $\Delta T_{corr(\beta=0)}$  is the temperature correction and  $\beta$  is the heating rate.

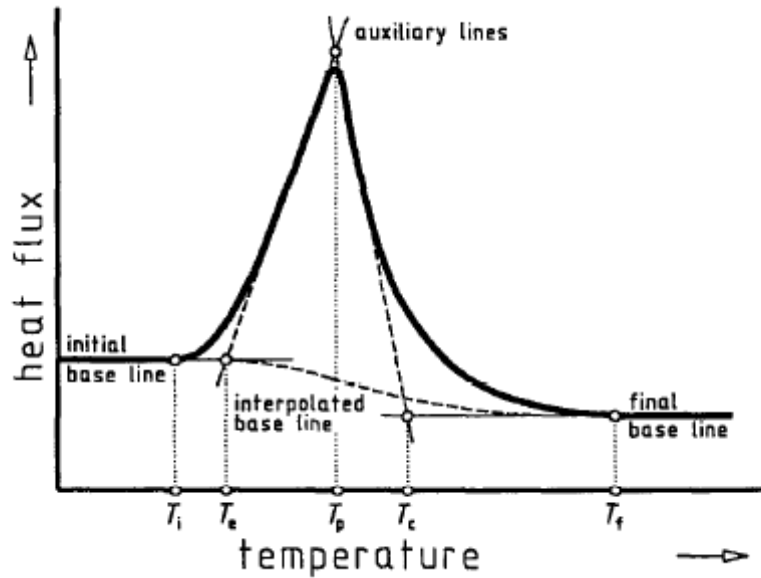


Figure 2-2 Definition of characteristic temperatures of a peak (Höhne *et al.*, 1990)

Rather than using the onset temperature, Schawe (1993) used the temperature corresponding to the initial phase transition time as the phase transition temperature. He argued that the heating rate was not constant during the phase transition process, thus the shape of DSC curve would be deformed.

It has been shown that the sample temperature measured at the heating rate of the calibration does represent the true temperature (Wu and Perepezko, 2000). In their work, the device was calibrated at 20°C/min by the ASTM method; after which the eutectic temperature of Co-18.5 at % Al was measured at various heating rates; Finally the true temperature for heating rates other than 20°C/min was obtained only after applying a secondary correction to the results. The heating rate used for calibration (20°C/min) obviously required no secondary correction factor (Figure 2-3).

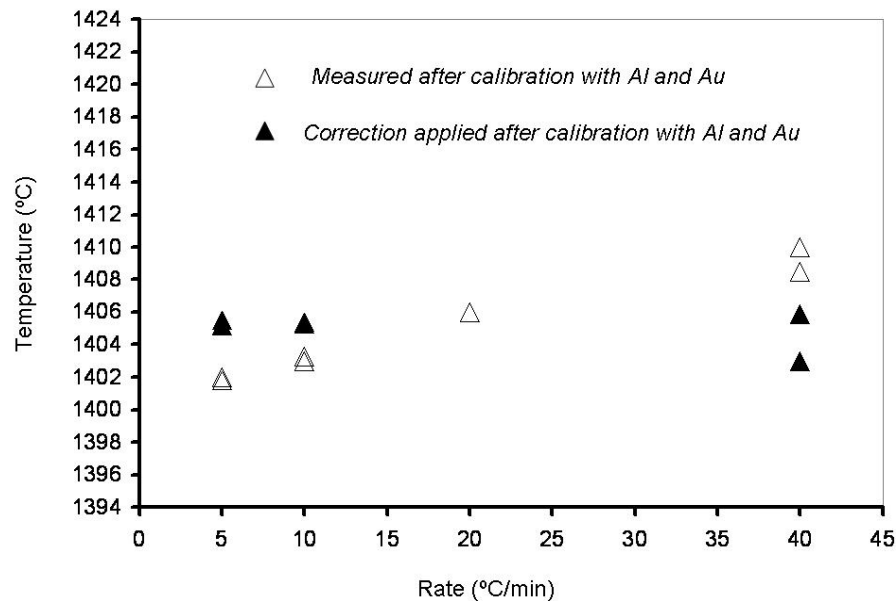


Figure 2-3 Results of the eutectic temperature of Co-18.5 at %Al after initial calibration and correction (Wu and Perepezko, 2000)

The effect of various experimental parameters on phase transition enthalpy measurements can be studied by using the heat calibration factor  $K_Q$ . The heat calibration factor is the ratio of the true enthalpy and the peak area on a time scale plot. GEFTA's results (Gmelin and Sarge, 1995) showed that the enthalpy calibration factor was influenced by both the heating rate and the sample mass (Figure 2-4).

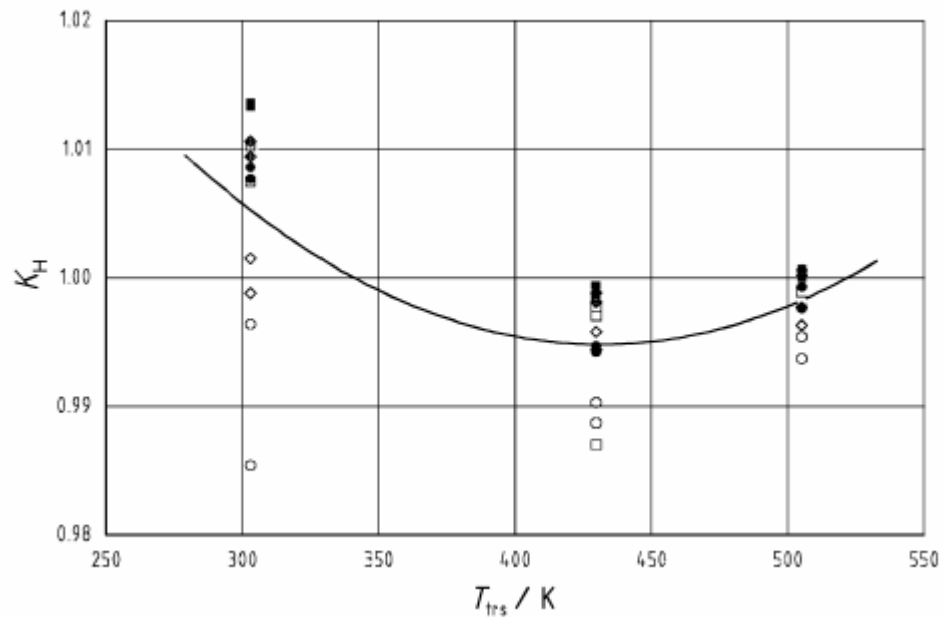


Figure 2-4 Enthalpy calibration factor plotted against transition temperature for gallium, indium and tin. (Gmelin and Sarge, 1995)

Open symbols:  $m \approx 3$  mg; solid symbols:  $m \approx 10$  mg. Circles:  $\beta = 1$  K min<sup>-1</sup>; diamonds:  $\beta = 5$  K min<sup>-1</sup>; squares:  $\beta = 10$  K min<sup>-1</sup>.

### 2.3. Effect of oxidation on specific heat capacity measurements

Differential Scanning Calorimetry (DSC) is not the only technique that can be used to measure specific heat capacity ( $C_p$ ). Other methods include the adiabatic method and the heat pulse (both electric and laser pulse) method (Bortfeldt and Kramer, 1991). However, its ability to perform continuous measurements distinguishes the DSC technique.

The oxidation of metal/alloy in heat capacity measurement using the DSC technique has been widely noted. Due to the limitations on the size of the sample mass that can be used in DSC measurements, sample oxidization becomes a significant factor in heat capacity measurements. In order to reduce this undesirable effect, Wang and Overfelt (2003) measured the heat capacity of magnesium alloys by separating the samples from the environment by sealing the BN coated sample with alumina powder into a crucible. Although the approach was successful, the process was complex and tedious. In particular, precautions had to be taken to protect the BN coating from flaking.

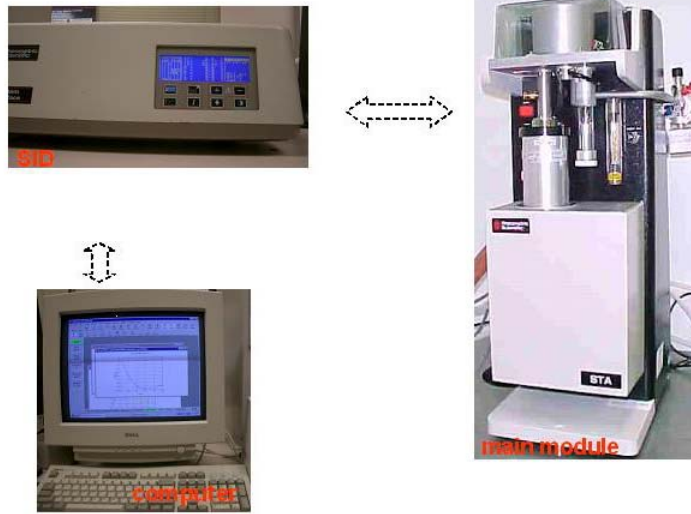
Theoretical calculations of the effect of oxidation based on existing thermodynamic knowledge were developed for this research. The contribution of the sample oxidation to heat capacity measurements can be quantified as to the amount of oxide generated and the formation enthalpy of the oxide released by the oxidation reaction. The effect of the amount of oxide generated on the measured signal is a mixture of that due to the pure element and that due to its oxide, while the enthalpy of the reaction weakened the true endothermic heat flow signal. The effect due to these two factors was studied based on a combination of the TGA results with those from DSC. Finally a correction curve was produced for the measured heat capacity results.

### **3. EXPERIMENTAL PROCEDURE AND ANALYTICAL TECHNIQUES**

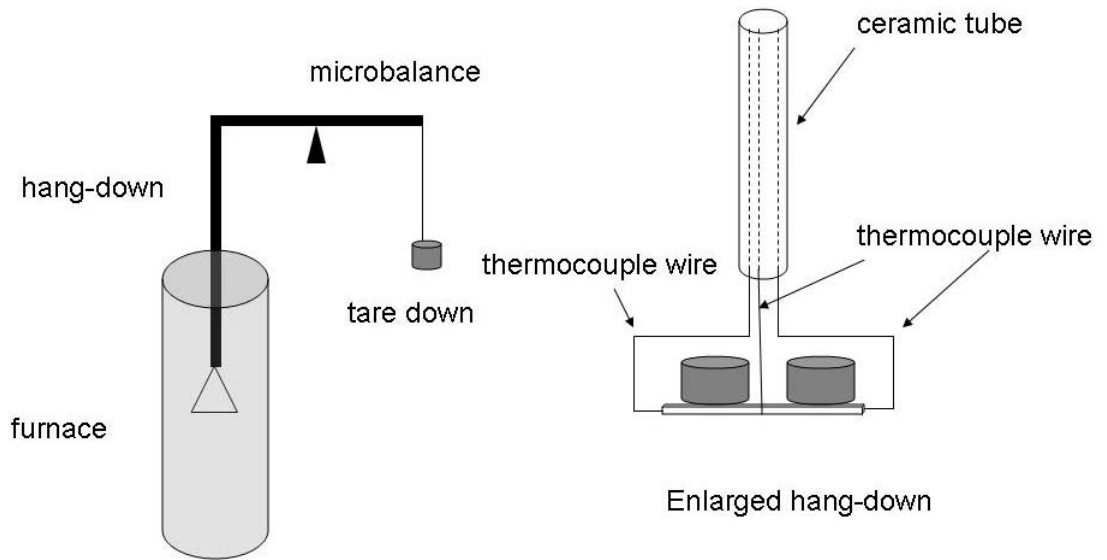
#### **3.1. Simultaneous Thermal Analysis 1500 (STA1500) instrument**

The Simultaneous Thermal Analyzer 1500 (STA-1500) (Rheometric Scientific Inc) combines a heatflux type Differential Scanning Calorimeter (DSC) with a Thermal Gravimetric Analyzer (TGA). A maximum measuring temperature of 1500°C can be achieved and the maximum sample size is 40mg. The equipment consists of three parts: the main module, the surface interface device (SID), and the computer system (Figure 3.1(a)).

The main module is where the experimental measurements are performed. Figure 3-1(b) shows a schematic of the structure of the main module. It is assembled by a moveable high temperature furnace, a microbalance, and a hang-down. The core part of the DSC is located at one end of the hand-down, where the sample/standard pan and reference pan are side by side on a Pt heatflux plate with a three-wire R type (Pt/Pt-13%Rh) thermocouple. The other end of the hang-down is attached to the microbalance from which the assembly is suspended makes it possible to record TGA and DSC measurements simultaneously.



(a)



Schematic of main module of STA

(b)

Figure 3-1 (a) Simultaneous Thermal Analyzer 1500 (Rheometric Scientific, Inc.),  
 (b) schematic drawing of the main module and the hang-down.

The SID (surface interface device) is used for signal acquisition and to control the heating program and interfaces the main module with the computer system. The computer system controls the results analysis and the experimental process.

### **3.2. Experimental set-up to determine the effects on phase transition temperature and enthalpy measurement**

#### **3.2.1. Determination of phase transition temperature**

Based on the DSC plot of the phase transition peak, five temperature points can be defined in a typical melting peak (Figure 3-2): peak temperature,  $T_p$ , which is the intersection point of two tangential lines extrapolated on both sides of the peak; the onset temperature,  $T_{on}$ , which is the intersection point from extending the peak's tangential lines with the extrapolated baseline at the lower temperature side; the offset temperature  $T_{off}$ ; which is the intersection point corresponding to  $T_{on}$  located on the higher temperature side; the initial temperature,  $T_i$ , which is the starting point for the phase transition; and the temperature at which the phase transition is complete, the final temperature,  $T_f$ .



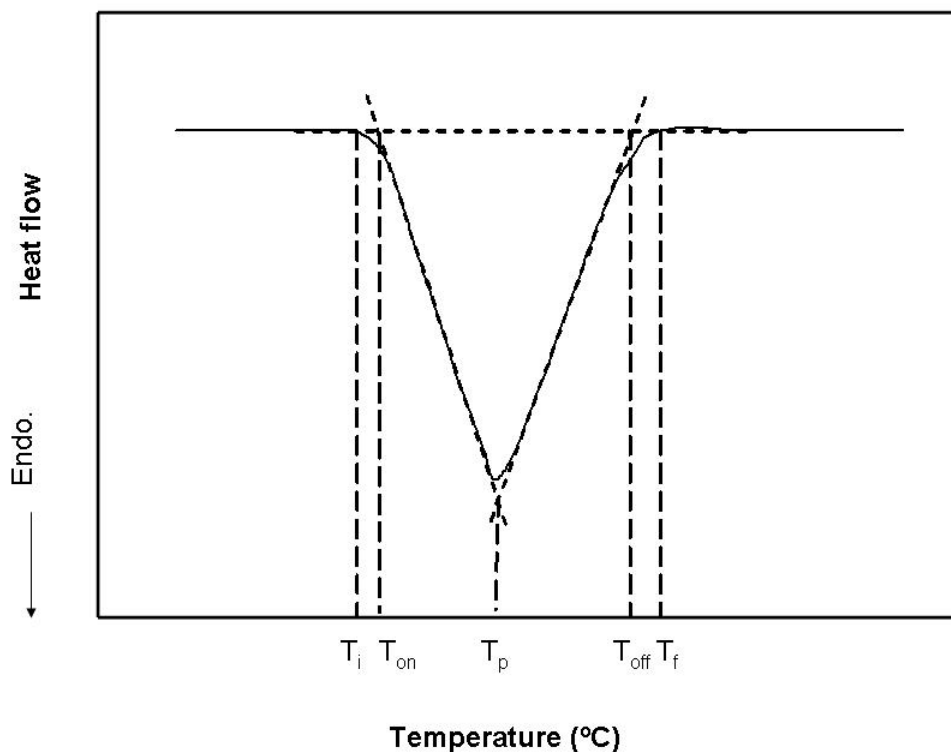


Figure 3-2 DSC trace for a typical melting peak per ASTM conventions

In general,  $T_i$ ,  $T_{on}$  and  $T_p$  are used in the literature. The merit of selecting the peak temperature  $T_p$  is that it can be defined in a very straightforward way. However, it suffers from considerable drift due to the sample properties (Cieslak et al., 1990; Cao et al., 1991; Sarri et al., 2003). Compared with the other two temperature points, the onset temperature is less influenced by the sample properties and so is often used (Price, 1995; Schubnell, 2000; Wang and Overfelt, 2003). However, Schawe (1993) pointed out that the nonlinear heating rate during the phase transition leads to some deformation of the melting peak and therefore suggested using the initial phase transition temperature as the measured temperature. The raw signal measured by STA in DSC mode and its first deviations are plotted in Figure 3-3. The first derivative of the heat flow vs. temperature

plot clearly shows that the left side of the peak is not linear. Consequently, the position of the tangent line to the left of the peak can not be precisely determined. This kind of uncertainty in the tangent line position leads to uncertainty in the onset phase transition temperature ( $T_{on}$ ) determination.

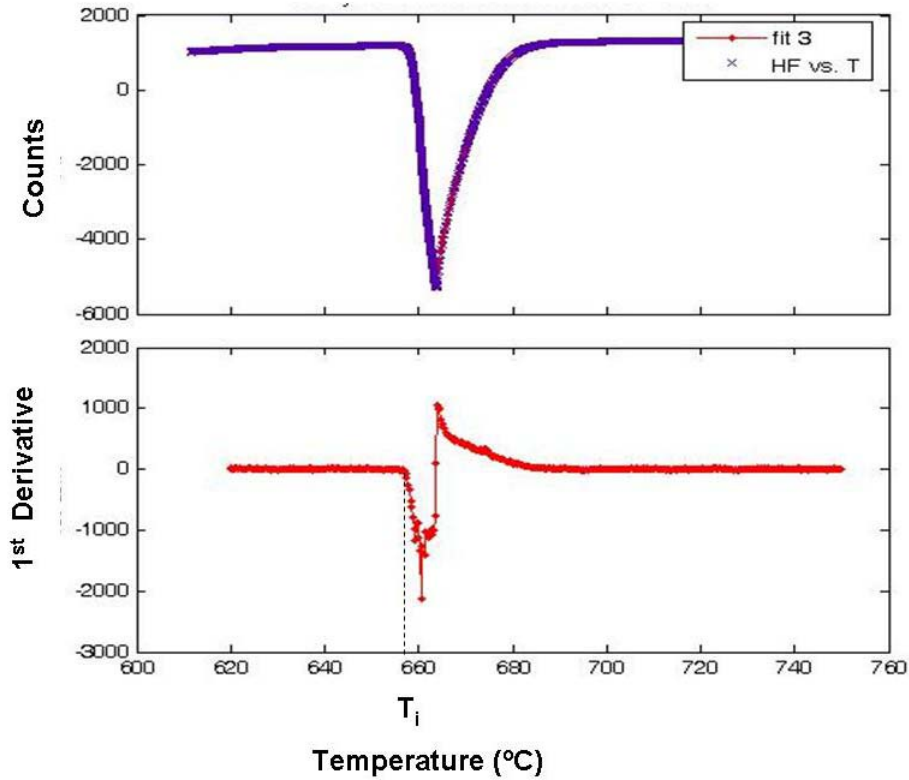


Figure 3-3 (a) Raw signal of STA in DSC mode, (b) First derivative of raw signal

In this research, the initial phase transition temperature ( $T_i$ ) was used as the measured melting temperature. Since there is no sharp transition at the initial temperature in the raw data, it is difficult to determine precisely where the starting point should be from the raw data. The use of the first derivative of the raw signal vs.

temperature was therefore adopted to determine the initial phase transition temperature,  $T_i$ .

### 3.2.2. Experimental set-up to determine the effects of experimental variables

All the experiments reported in this section utilized the calibration mode of the STA1500. The micro-balance was zeroed before each experiment.

#### 1) Heating rate effect

The major steps consisted of:

- a) **Sample preparation:** all the pellet samples were prepared from high purity rod metals. Aluminum and zinc rods (99.999%, Alfa, metal base) with diameters of 4.0mm were sliced using a diamond saw then ground and polished on both sides to achieve the desired thickness. Finally, the samples were cleaned with ethanol and air dried before loading. The alumina crucibles for both sample and reference were covered with lids.
- b) **Experimental procedure:** A step-temperature program was used for the melting point and transition heat study:
  - i) heating from room temperature to a temperature lower than the melting point (zinc 380°C or aluminum 610 °C) at the maximum heating rate;
  - ii) a dwell time of 10 minutes for equilibration;
  - iii) continuous heating at the desired heating rate (2, 5, 10, 20, or 35°C/min) to a temperature above the melting point (460°C for zinc or 750°C for aluminum);

iv) once the maximum setting temperature was reached, the furnace automatically shut down.

The instrument is cooled by recirculating water at 22°C throughout.

The experimental conditions tested to examine the effect of different heating rates are listed in Table 3-1. The powder samples were used to investigate the effect of combining factors.

Table 3-1 Experimental design to examine the effect of heating rate on the phase transition temperature

	Heating rate (°C/min)				
	2	5	10	20	35
<b>Aluminum pellet, 9.6mg</b>	√	√	√	√	√
<b>Zinc pellet, 9.6mg</b>	√	√	√	√	√

√ corresponds to conditions tested

## 2) Sample geometry effect

The aluminum samples with three particle size distributions were prepared. The particle size distributions were measured using a laser particle size analyzer, Microtrac 3500. Figure 3-4 gives the results of the particle size distribution measurements. Since the particle size distribution for powder1500 was outside the range of the laser particle size analyzer, an optical microscope was used and the distribution of particle based on counting results. Table 3-2 summarizes the particle size distributions. The mean particle size diameters for aluminum37, aluminum112 and aluminum1500 are: 37µm, 112µm and 1500µm, respectively.

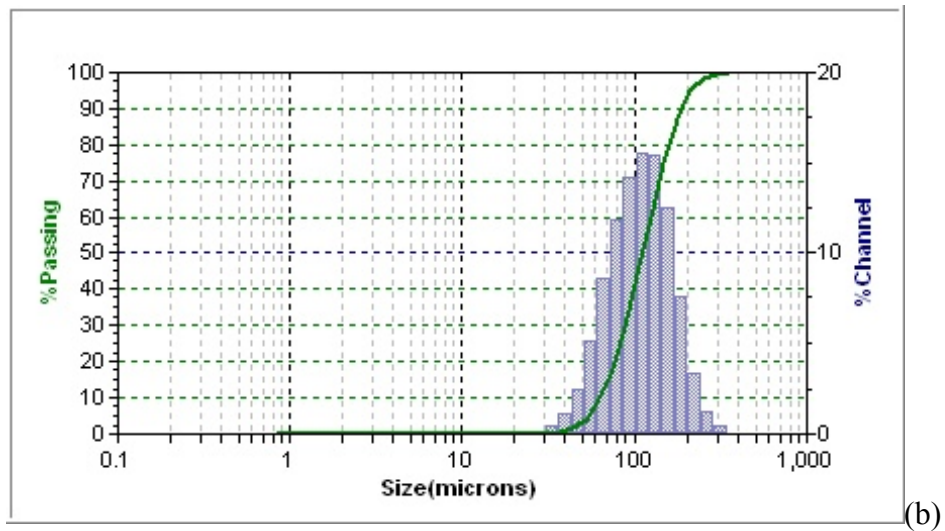
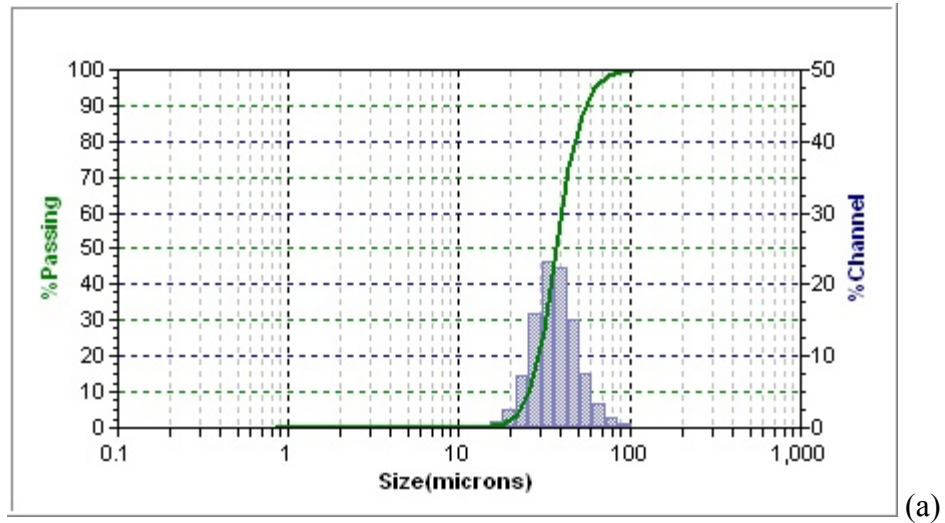


Figure 3-4 Particle size distribution of a) powder37, (b) powder112

Table 3-2 Particle size distributions of aluminum powder samples

% (wt)	Diameter ( $\mu\text{m}$ )	
	Powder37	Powder112
10	25.71	63.36
20	29.18	76.56
30	31.93	88.28
40	34.44	99.91
<b>50</b>	<b>36.99</b>	<b>112.0</b>
60	39.82	125.2
70	43.11	139.8
80	47.52	157.9
90	54.83	185.0
95	62.38	209.9

### 3) Mass effect

Three mass sizes (9.6mg, 20mg and 30 mg) and four geometry types (three powders with different particle size distributions and one pellet aluminum sample) were used in this study. The temperature program was the same as in previous experiments. Table 3-3 summaries the experiments conducted for each set of experimental conditions.

Table 3-3 Experimental designs to examine the effect of sample mass

	Mass(mg)	Heating rate (°C/min)	
		10	20
<b>Aluminum pellet</b>	9.6	☺	☺
	20	☺	√
	30	☺	√
<b>Aluminum37</b>	9.6	☺	√
	20	☺	√
	30	☺	√
<b>Aluminum112</b>	9.6	-	☺
	20	-	√
	30	-	√
<b>Aluminum1500</b>	9.6	-	☺
	20	-	√
	30	-	√

☺ done in heating rate effect experiments; √ mass effect experiments;

- experiments not performed

### 3.2.3. Experimental set-up for sensitivity calibration

Sensitivity calibration is a necessary step to convert the raw signal measured into the heat flow (heat per unit time). The raw signal measures the temperature difference between the reference (here, an empty pan) and the sample, and is expressed as an electrical voltage. There are two major steps in the sensitivity calibration, namely

- 1) Zeroline line measurement, where the empty sample crucible is measured
- 2) Standard sample measurement, where a standard sapphire disc is measured

A continuous-temperature program was used for sensitivity calibration. The sensitivity calculation was performed using the instrument's software. The effect of heating rate on the sensitivity calibration was studied using the same procedure for different heating rates.

#### 3.2.4. Calculation of the heat calibration factor

The heat calibration factor can be applied to correct the measured phase transition enthalpy from the DSC results. The heat calibration factor  $K_Q$  is defined as the ratio of the true phase transition enthalpy and the peak area of standard samples in a time scale plot, that is:

$$K_Q = \frac{Q_{true, std}}{A_{std}} \quad (3-1)$$

For a sample with an unknown phase transition enthalpy, the phase transition enthalpy per unit mass can be calculated as:

$$q_s = K_Q * \frac{A_s}{m_s} \quad (3-2)$$

Where  $A_s$  and  $m_s$  are the peak area and mass of the unknown sample.

The peak area can be calculated by extrapolating a linear baseline along the heat flow of solid and liquid, then integrating to obtain the area under the curve. Figure 3-5 shows typical heat flow peak areas.



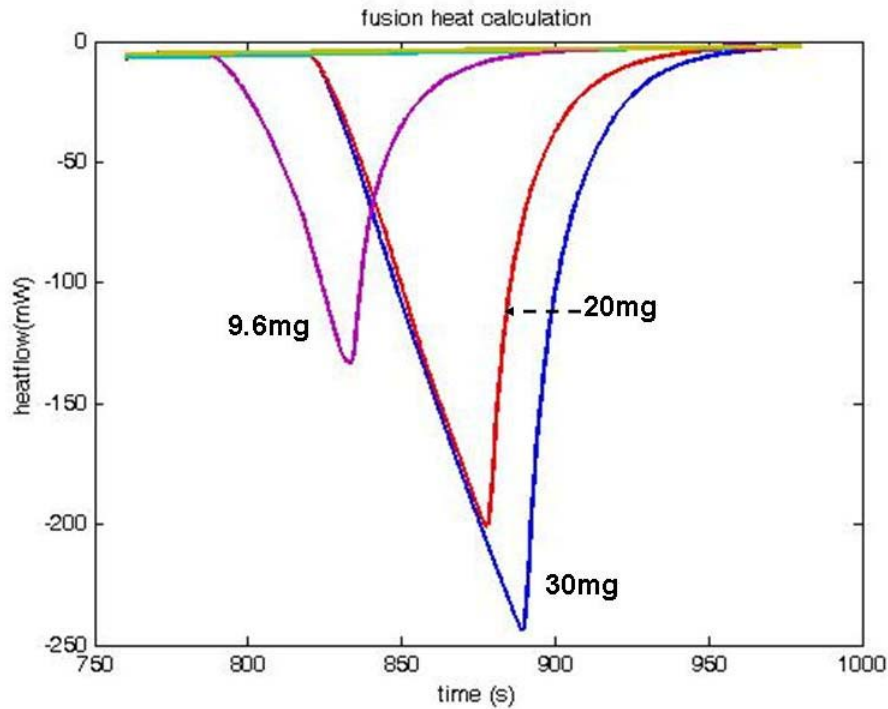


Figure 3-5 Peak areas calculation of aluminum pellet samples

### 3.3. Effect of oxidation on specific heat capacity ( $C_p$ ) measurements

#### 3.3.1. Experimental set-up for $C_p$ measurement

In this section, all the experiments were carried out using the normal operation mode of the STA1500. 20mg aluminum pellets and 20mg of aluminum powders with a mean diameter of  $37\mu\text{m}$  were measured. The following temperature program was utilized:

- i) dwell at  $28^\circ\text{C}$  for 5 minutes;
- ii) ramp up to  $710^\circ\text{C}$  at a heating rate of  $20^\circ\text{C}/\text{min}$ ;

High purity argon gas at  $50\text{ml}/\text{min}$  was flowed through the measuring chamber and  $22^\circ\text{C}$  cooling water was used through the measurement.

### 3.3.2. Method for calculating $C_p$ from DSC results

Based on the definition of specific heat capacity ( $C_p$ ,  $\text{J g}^{-1} \text{ }^\circ\text{C}^{-1}$ ), the basic equation for  $C_p$  measurement is:

$$dQ = m * C_p * dT \quad (3-3)$$

Where  $dQ$  is the heat absorption for a sample temperature change  $dT$  due to the heating process;  $m$  is the sample mass, and  $C_p$  is a function of the temperature under constant pressure.

For DSC, the relationship between heat flow  $\frac{dQ}{dt}$  and  $C_p$  is:

$$\frac{dQ}{dt} = m * C_p * \frac{dT}{dt} \quad (3-4)$$

A general comparison method is used to measure  $C_p$  in the DSC technique. Besides the sample, this requires a standard sample (e.g. a standard sapphire disc,) to be measured under the same experimental conditions as the specimen. The heat capacity of the unknown specimen can then be calculated using the equation:

$$C_{p,s} = \frac{\frac{dQ}{dt}^s}{\frac{dQ}{dt}^{std}} * \frac{m_{std}}{m_s} * C_{p,std} \quad (3-5)$$

However, due to the limitations of the practical measuring process, the measured heat flow signal includes heat flow from both the sample and the crucible. Therefore, a conventional three-step  $C_p$  measurement method must be used. Figure 3-6 shows the three-step method used for heat capacity measurements.

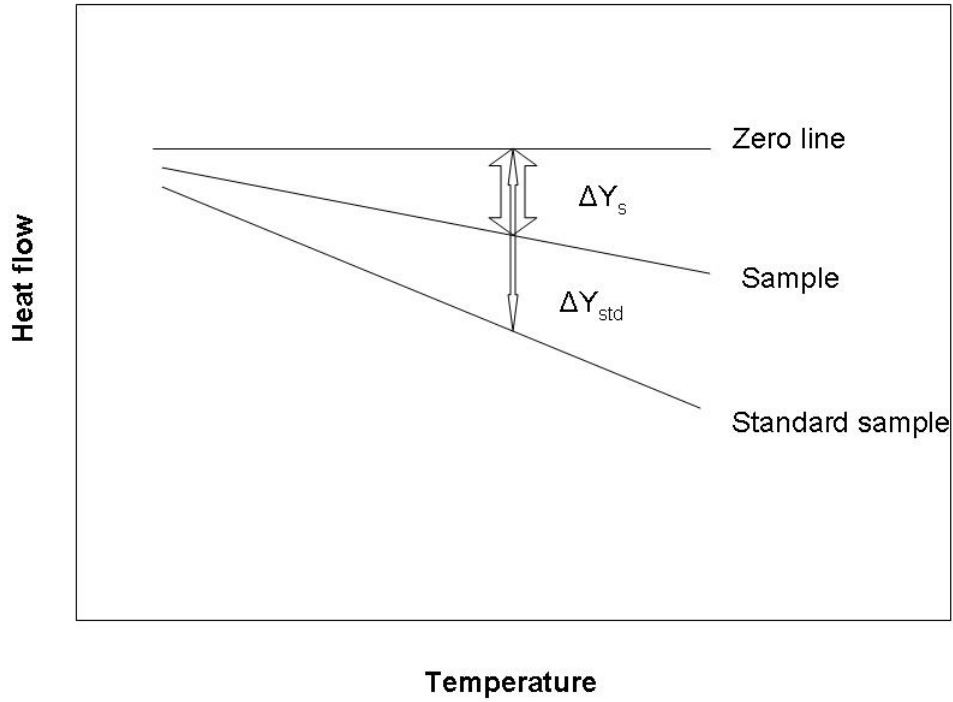


Figure 3-6 Heat capacity measurements using the conventional three-step method

The three-step method used in heat capacity measurements consists of the following steps:

- i) a zeroline measurement on the empty crucible
- ii) the standard sample measurement
- iii) the unknown sample measurement

Therefore, Equation (3-5) becomes

$$C_{p,s} = \frac{\Delta y_s}{\Delta y_{std}} * \frac{m_{std}}{m_s} * C_{p,std} \quad (3-6)$$

Here

$$\Delta y_s = \frac{dQ}{dt}_{,s} - \frac{dQ}{dt}_{,z}; \quad (3-7)$$

$$\Delta y_{std} = \frac{dQ}{dt}_{,std} - \frac{dQ}{dt}_{,z} \quad (3-8)$$

The subscript “z” denotes the empty crucible measurement, “std” is the standard sample, and “s” is the sample

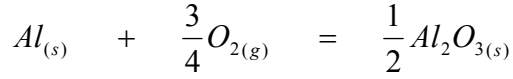
### 3.3.3. Calculation of the generated oxide effect on $C_p$ measurement

The metal oxide was generated during the  $C_p$  measurement process due to oxidation of the metal sample. So the measured  $C_p$  should be the  $C_p$  of the mixture of pure metal and its oxide, and it can be expressed as:

$$C_{p,mixture} = C_{p,metal} * \%M + C_{p,oxide} * \%MO \quad (3-9)$$

Here,  $C_{p,metal}$  and  $C_{p,oxide}$  are specific heat capacity of the metal and its oxide, respectively.  $\%M$  and  $\%MO$  are the weight percentage of metal and its oxide in the mixture.

Since both  $C_{p,metal}$  and  $C_{p,oxide}$  are known and there is the relationship between  $\%M$  and  $\%MO$ , which is  $\%M = 100 - \%MO$ , the crucial step is to determine the weight percentage of metal oxide ( $\%MO$ ) that is present during the measuring process. Assuming that the total mass increase during the  $C_p$  measurement is only due to the metal oxidation, the amount of the generated oxide therefore can be obtained as the following:



$$1mol * 27g/mol + \frac{3}{4}mol * 32g/mol = \frac{1}{2}mol * 102g/mol = 51g$$

That means when the total mass changes by 24g, 51g of aluminum oxide has been generated and 27g of aluminum has been consumed. Based on the total mass change  $\Delta m_{total}$  from the TGA results, the mass of generated aluminum oxide can be gotten from:

$$m_{Al_2O_3} = \frac{50.97}{24} * \Delta m_{total} (g) \quad (3-10)$$

Thus, the weight percentage of the metal oxide is:

$$\%MO = \frac{m_{MO}}{m_{total}} * 100\% \quad (3-11)$$

Furthermore, the effect on the  $C_p$  measurement due to a given amount of generated oxide can be easily derived by:

$$\alpha = \frac{C_{p,mixture} - C_{p,pure}}{C_{p,pure}} * 100\% \quad (3-12)$$

### 3.3.4. Calculation of the effect of oxidation reaction enthalpy on $C_p$ measurement

The exothermic oxidation reaction counteracts the endothermic heat capacity measurement in heating and melting processes. Therefore, the true heat flow signal from the metal sample is reduced by the reaction enthalpy released by the oxidation reaction.

In this paper, a method is proposed to calculate the effect of the oxidation reaction heat on the heat capacity measurement based on thermodynamics. This method converts the oxidization reaction enthalpy into a heat flow signal, then evaluates the effect of the oxidization reaction on the  $C_p$  measurement and finally applies the appropriate correction to the measured results. The method consists of three major steps: 1) calculating the reaction enthalpy at each temperature for the entire measurement range; 2) converting the reaction enthalpy into the form of a heat flow signal; 3) evaluating the effect of the reaction enthalpy on the heat capacity measurement.

### 1) Reaction enthalpy calculation

The standard reaction enthalpy at room temperature  $\Delta H_f^{298}$  (1675.7KJ/mol) can be easily found in literatures (Van Wylen and Sonntag, 1986; Gaskell, 1995). Other than the room temperature, the reaction enthalpy (KJ/mol) can be calculated from:

$$\Delta H_f^T = \Delta H_f^{298} + A * t + \frac{B * t^2}{2} + \frac{C * t^3}{3} + \frac{D * t^4}{4} - \frac{E}{t} + F - H \quad (3-13)$$

Here  $t = \text{temperature (K)}/1000$ , the coefficients of  $A, B, C, D, E, F$  and  $H$  are listed in Table 3-4.

Table 3-4 Coefficients of the reaction enthalpy (NIST, 2005)

	<i>A</i>	<i>B</i>	<i>C</i>	<i>D</i>	Temperature range (K)
<b>Al<sub>2</sub>O<sub>3</sub> (<math>\alpha</math> phase)</b>	102.49	38.7498	-15.9109	2.62818	298-2327
	<i>E</i>	<i>F</i>	<i>H</i>		
	-3.007551	-1717.930	-1675.690		

## 2) Conversion from reaction enthalpy to heat flow

The reaction enthalpy can be converted to a heat flow signal using the following equation:

$$\left. \frac{dH}{dt} \right|_{\text{reaction}} = \frac{dH}{dm} * \frac{dm}{dt} \quad (3-19)$$

Here

$$\frac{dH}{dm} (J/g) = d \left( \frac{\Delta H}{m} \right) = \frac{\Delta H_f^T (J/mol)}{101.98 (g/mol)} = \frac{\Delta H_f^T}{101.98} (J/g) \quad (3-20)$$

$\frac{dm}{dt}$  is the generated oxide mass per unit time and can be obtained from the first derivative of the oxide mass vs. time plot.

## 4. RESULTS AND DISCUSSION

### 4.1. Melting point temperature measurements

#### 4.1.1. Analysis of raw experimental results

High purity aluminum and zinc pellets were measured for a range of heating rates: 2, 5, 10, 20, 35°C/min. The raw data were plotted against both time and temperature and the results are shown in Figure 4-1 (aluminum) and Figure 4-2 (zinc).

The effect of the heating rate on the phase transition peak can be described in terms of the peak position and the peak shape, which includes the sharpness of the peak and its overall width.

Examining the melting peak time scale plot reveals that the entire melting peak shifts left towards shorter times as the heating rate increases. This is as expected, since samples with higher heating rates need less time to reach the melting point. However, the effect of the heating rate shown on the temperature scale plot reveals that the shift in the peak position is significant as the initial phase transition temperature, onset temperature and peak temperature all appear to shift slightly towards higher temperatures as the heating rate increases. This has been ascribed to the samples experiencing greater temperature gradients from the higher heating rates (Speyer, 1994).



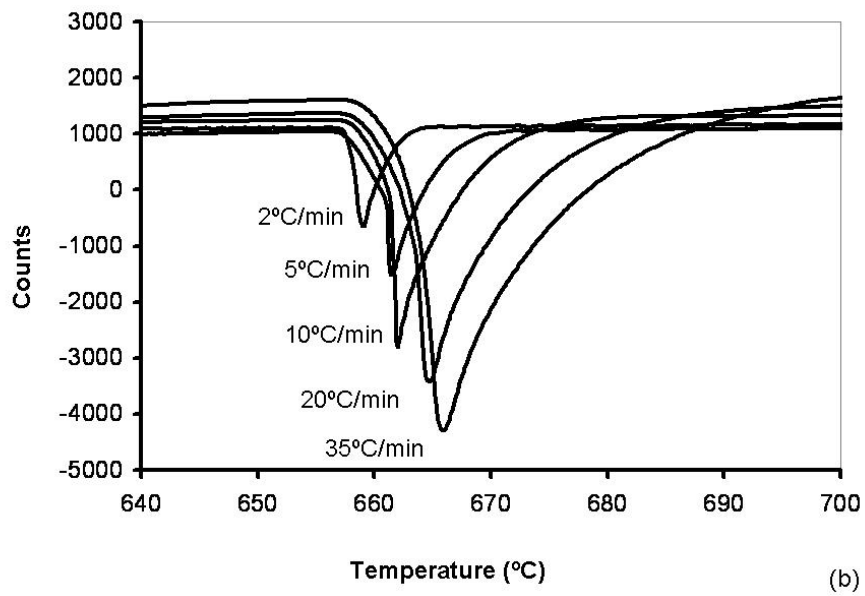
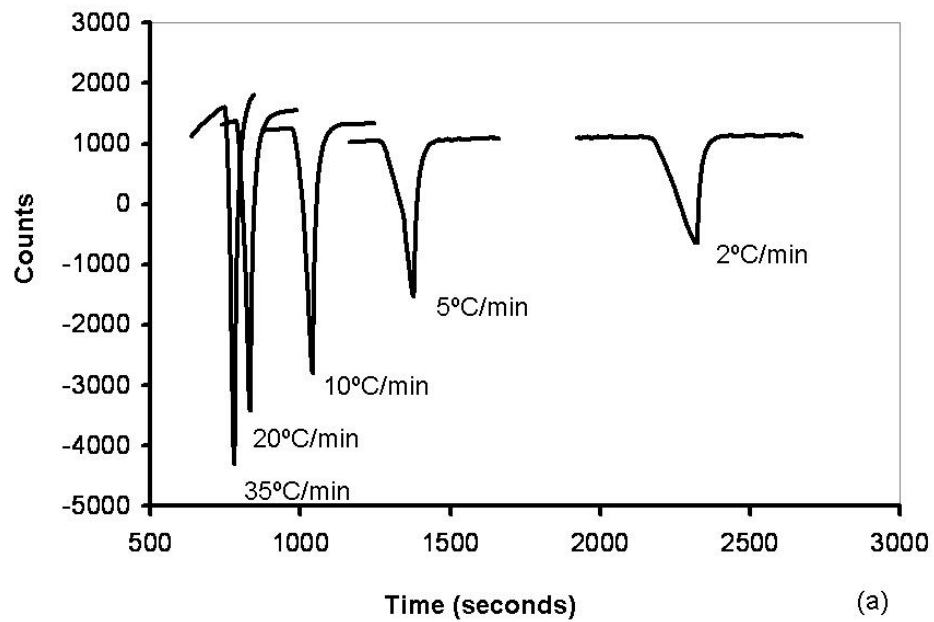


Figure 4-1 Raw data for aluminum pellet samples with varying heating rate as a function of (a) time, (b) temperature ( $T_m=660.1^\circ\text{C}$ )

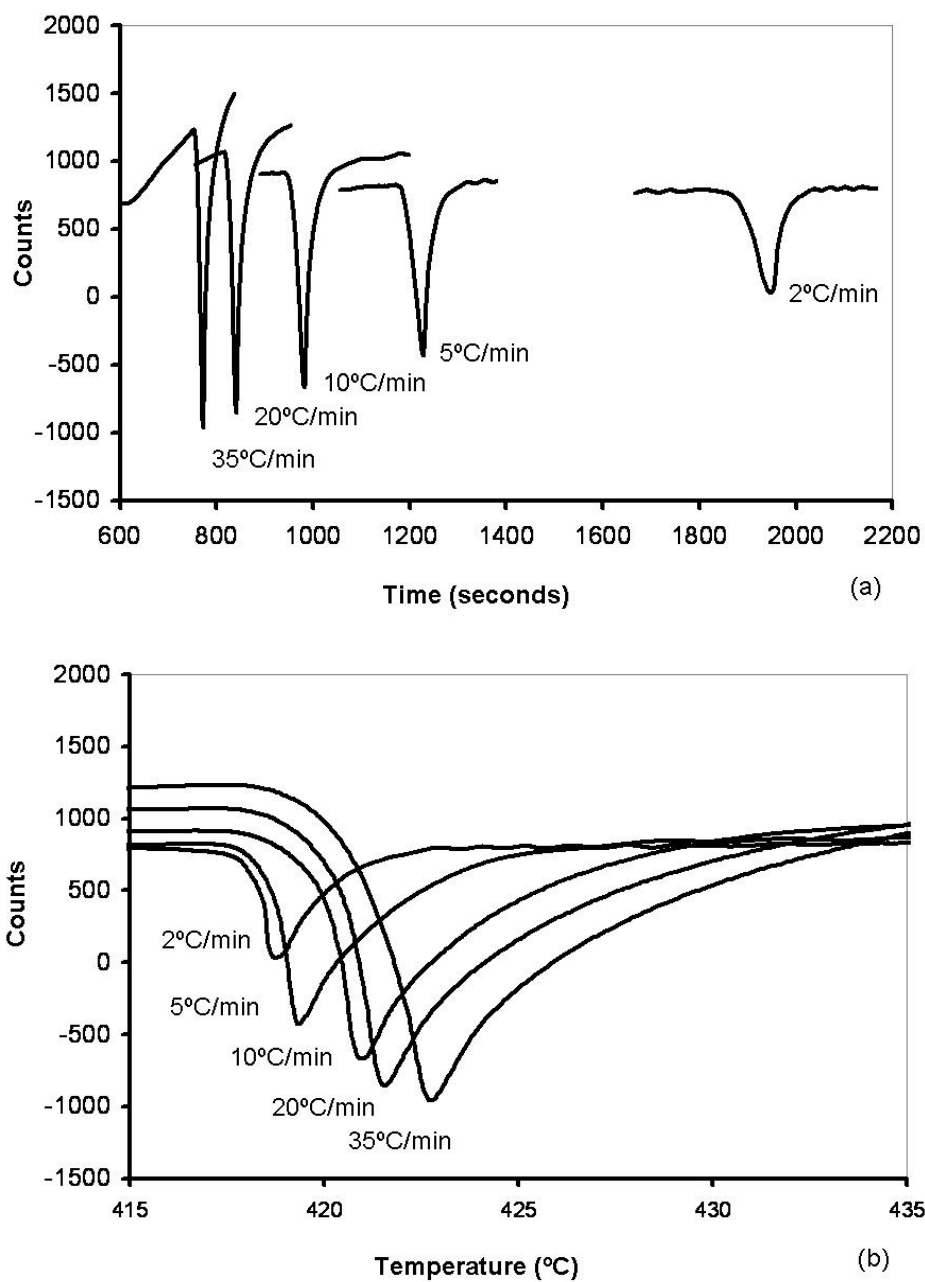


Figure 4-2 Raw data for zinc pellet samples with varying heating rate as a function of (a) time, (b) temperature ( $T_m=419.5^\circ\text{C}$ )

The peak minima increase as the heating rate increases in both time and temperature scale plots. Based on the principles of DSC, the peak minimum corresponds to the greatest electric potential signal difference (i.e. temperature difference) between the reference and the sample. Even though both the sample and reference temperatures continue to increase during the phase transition process, a significant temperature difference can be detected because the melting process slows the increase in the sample temperature while the reference temperature continues to increase at the setting heating rate. This temperature difference becomes even more significant as the heating rate increase, so the peak sharpness increases with increasing heating rate.

The width of the peak shows opposite trends in the temperature scale plot and the time scale plot; the peaks become narrower in the time scale plot and broader in the temperature plot as the heating rate increases. The peak width in the time scale corresponds to the phase transition time interval. The higher heating rate means a greater heat flux into the sample hence a shorter phase transition time interval is needed. In contrast, the temperature scale plots reveal that the final phase transition temperature increases with the heating rate increase, which indicates that a higher process temperature is needed for the sample temperature to reach the reference temperature at higher heating rates. This is because a greater temperature difference exists between the sample and reference due to the higher heating rate.

In summary, higher heating rates appear to be more sensitive to the phase transition involved in the heating process, as indicated by the minima of peaks increasing with heating rate. However, this may cause an overlap of two phase transition peaks in close proximity because the peaks are broadened by faster heating rate.

#### 4.1.2. Effect of heating rate on the phase transition temperature

The phase transition temperature at various heating rates was determined using the first derivative method and listed in Table 4-1. The effect of the heating rate on the phase transition temperature is plotted in Figure 4-3.

Table 4-1 Phase transition temperatures of zinc and aluminum

Heating rate	Zinc (°C)			Aluminum (°C)		
	$T_p$	$T_{on}$	$T_i$	$T_p$	$T_{on}$	$T_i$
<b>2</b>	418.5	418.3	417.5	658.5	657.9	657.3
<b>5</b>	419.1	418.7	417.6	661.3	660.6	657.4
<b>10</b>	421.0	420.2	417.9	661.8	661.3	657.7
<b>20</b>	421.6	420.4	418.2	664.7	663.2	658.3
<b>35</b>	422.8	421.1	418.7	666.0	663.6	659.5
<b>Average</b>	420.6	419.7	417.9	662.5	661.3	658.0
<b>Std. dev.</b>	<b>1.7</b>	<b>1.2</b>	<b>0.5</b>	<b>2.9</b>	<b>2.3</b>	<b>0.9</b>

Compared with the peak temperature ( $T_p$ ) and the onset temperature ( $T_{on}$ ), the initial phase transition temperature ( $T_i$ ) has the smallest standard deviation.  $T_i$  is thus more reliable than  $T_p$  or  $T_{on}$  and should be used to represent the phase transition temperature.

The initial phase transition temperature shifts towards higher temperatures with increasing heating rate. The greater temperature gradient per unit time under the faster heating rate shifts the initial phase transition temperature towards the higher temperature range. This general trend in the heating rate data agrees with Höhne et al.'s research (Höhne et al., 1990). Although Wu and Perepezko (2000) found that the measured onset

temperature at 20°C/min heating rate is closest to the true melting temperature, this could not be confirmed based on the aluminum measurements reported here.

Linear least square is used for  $T_p$ ,  $T_{on}$  and  $T_i$  curve fitting (Figure 4-3). Their phase transition temperature differences at heating rate of zero are less than 1°C, which indicates that this temperature is close to the equilibrium phase transition temperature.

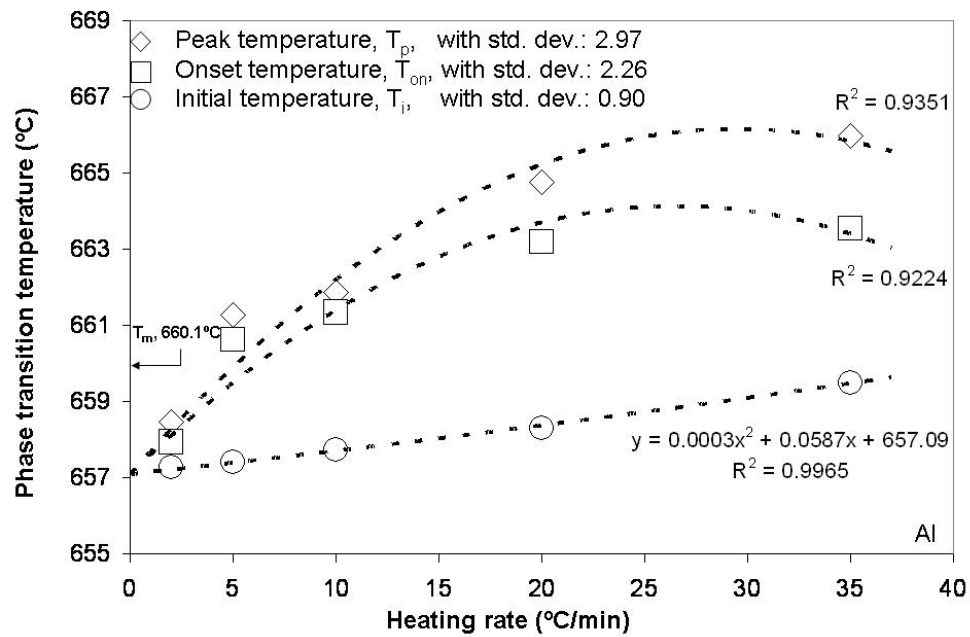
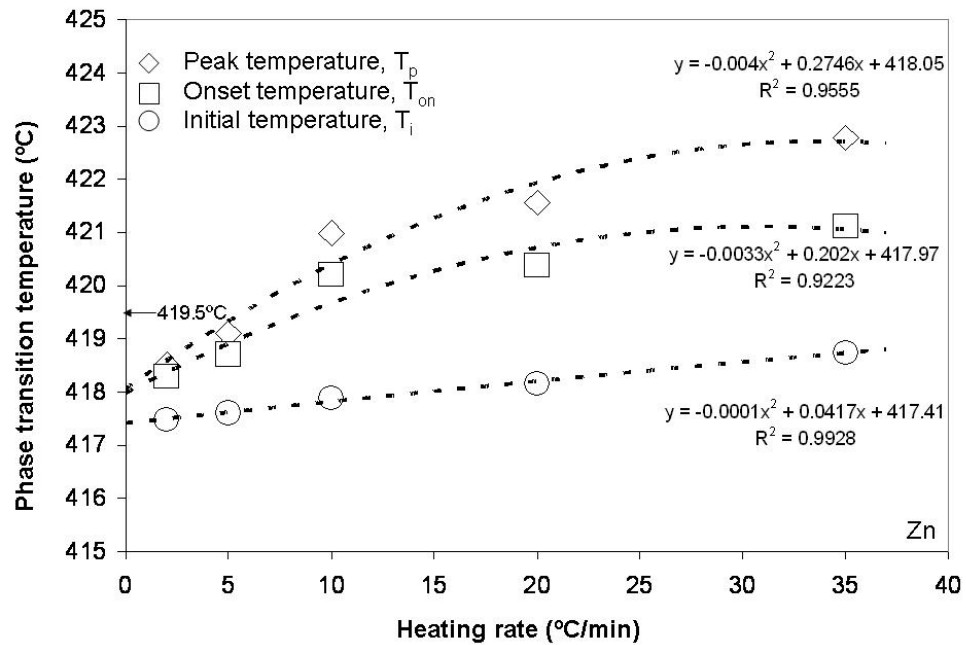


Figure 4-3 Initial phase transition temperature as a function of the heating rate  
 (a) zinc pellets; (b) aluminum pellets

The temperature calibration curve is plotted based on the measurements from both the zinc and aluminum standard samples in Figure 4-4. First, the initial phase transition temperature is found for heating rate at zero from the intercept of the extrapolated linear trendline on Figure 4-3. The temperature correction factor,  $\Delta T_{\text{corr}}(\text{heating rate}=0)$ , is then calculated based on the definition as:

$$\Delta T_{\text{corr}}(\beta = 0) = T_{\text{true}} - T_i(\beta = 0)$$

Where,  $T_{\text{true}}$  is the true melting point temperature of the pure element, either aluminum or zinc here, and the temperature correction factors for zinc and aluminum are listed in Table 4-2. Finally, the temperature correction factor was plotted vs. the measured initial phase transition temperature and the results shown in Figure 4-4.

Table 4-2 Temperature correction factors

	<b>T<sub>m</sub></b> <b>(°C)</b>	<b>T<sub>i</sub> (heating rate =0)</b> <b>(°C)</b>	<b>ΔT<sub>corr</sub> (heating rate=0)</b> <b>(°C)</b>
<b>zinc</b>	419.5	417.4	2.1
<b>aluminum</b>	660.1	657.2	2.9

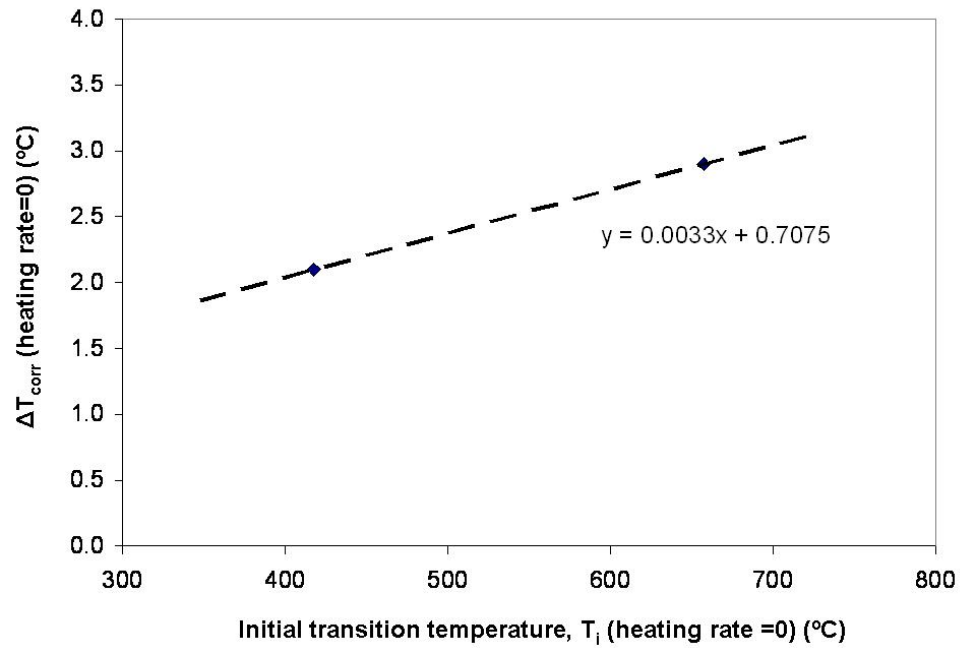


Figure 4-4 Temperature correction curve for pellet samples

According to the temperature correction curve in Figure 4-4, the true phase transition temperature between 417.4°C and 657.2°C can be obtained by applying the correction temperature  $\Delta T_{\text{corr}}(\text{heating rate}=0)$  to the experimentally measured temperatures.



### **4.1.3. Effect of sample mass on phase transition temperature**

Aluminum pellets with the same diameter but various mass sizes: 9.6mg, 20mg and 30mg were studied at heating rates of rate 10°C/min and 20°C/min, separately. Figure 4-5 shows raw results as a function of the sample mass.

The melting peak becomes broader and sharper, and the peak minimum shifts towards higher temperature with increasing sample mass. The phase transition enthalpy is proportional to the sample mass, so the time interval for the phase transition should become longer with increasing sample mass at a constant heating rate. A longer phase transition time interval means that the sample temperature will catch up with the reference temperature at higher temperatures, so the transition peak will become broader. At the same time, the maximum temperature difference between the sample and the reference increased and shifts to higher temperatures.

These results suggest that there is a certain minimum sample size required to detect the phase transition peak in the heating process, but too large a sample may cause close phase transition peaks to overlap due to broadening effects as discussed earlier.

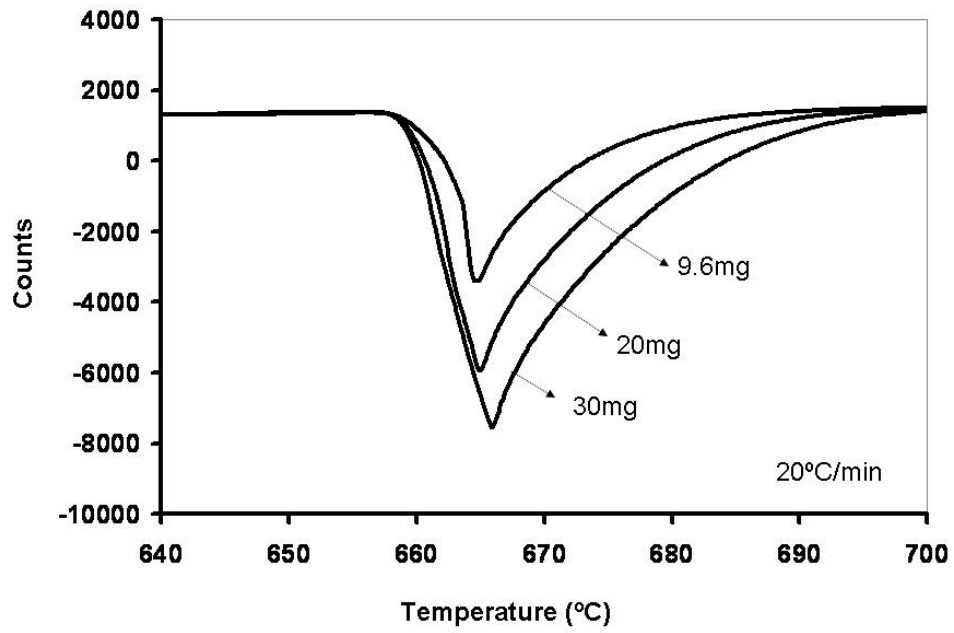
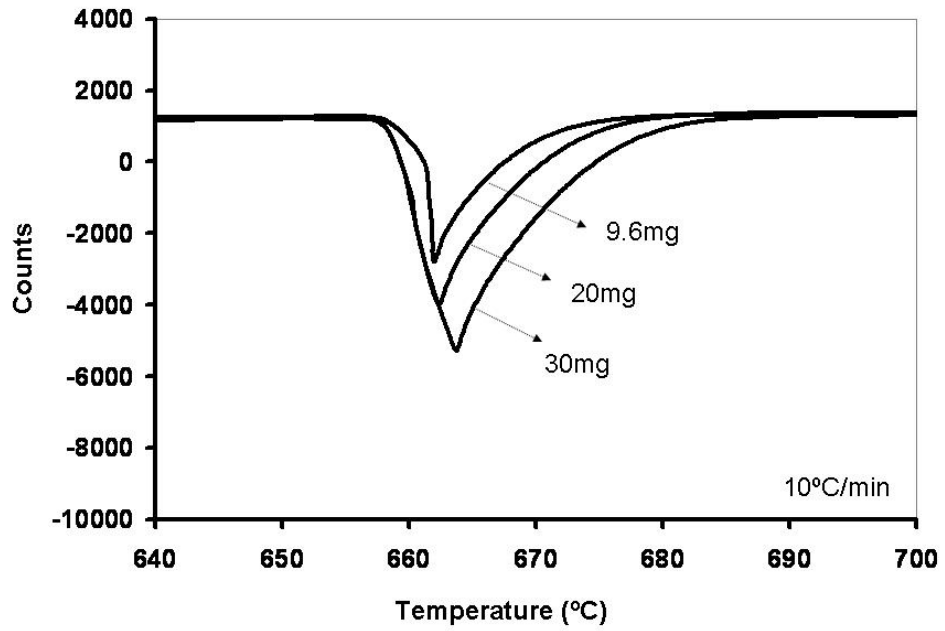


Figure 4-5 Raw results for aluminum pellets with varying mass size at the indicated heating rates

Compared with the effect of different heating rates, the effect of the sample mass on the initial transition temperature is insignificant in the raw results plot in Figure 4-5. Once again it was necessary to use the first derivative method to determine the initial phase transition temperature and the results are summarized in Table 4-3. Although the initial transition temperature shows a 0.6°C difference between the two heating rates of 10°C/min and 20°C/min, the effect of the sample mass size at a constant heating rate is insignificant (Figure 4-6). The standard deviation of the measured temperature from the average is 0.067 at heating rate 10°C/min, and 0.071 at the heating rate 20 °C/min, which agrees with the results reported in the literature (Breuer and Eysel, 1982; Höhne et al., 1990; Kalantary et al., 1995).

Table 4-3 Initial transition temperature for samples with different masses under heating rates of 10 °C/min and 20 °C/min

	<b>Initial transition temperature (°C)</b>	
	<b>10°C/min</b>	<b>20°C/min</b>
<b>9.7mg</b>	657.7	658.3
<b>20mg</b>	657.6	658.3
<b>30mg</b>	657.7	658.4
<b>Average</b>	657.7	658.3
<b>Std. dev.</b>	<b>0.067</b>	<b>0.071</b>

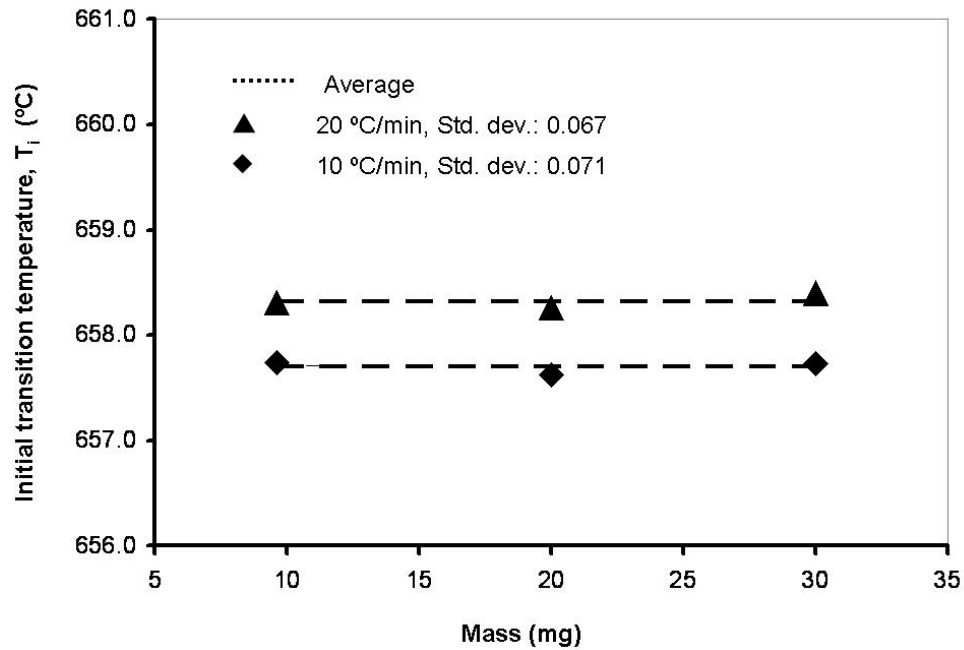


Figure 4-6 Initial phase transition temperature of aluminum pellet samples as a function of mass size (uncorrected data)

The combination of mass and heating rate effect was studied by plotting the initial phase transition temperature vs. heating rate (Figure 4-7). From linear least squares curving fitting of the initial phase transition temperature for aluminum, the  $T_i$  at heating rate of zero was determined to be 657.2°C, which is same as the previous result only considering the effect of heating rate. Therefore, the effect of the sample mass (10-30mg) on the initial transition temperature measurement for a pellet sample can safely be neglected.

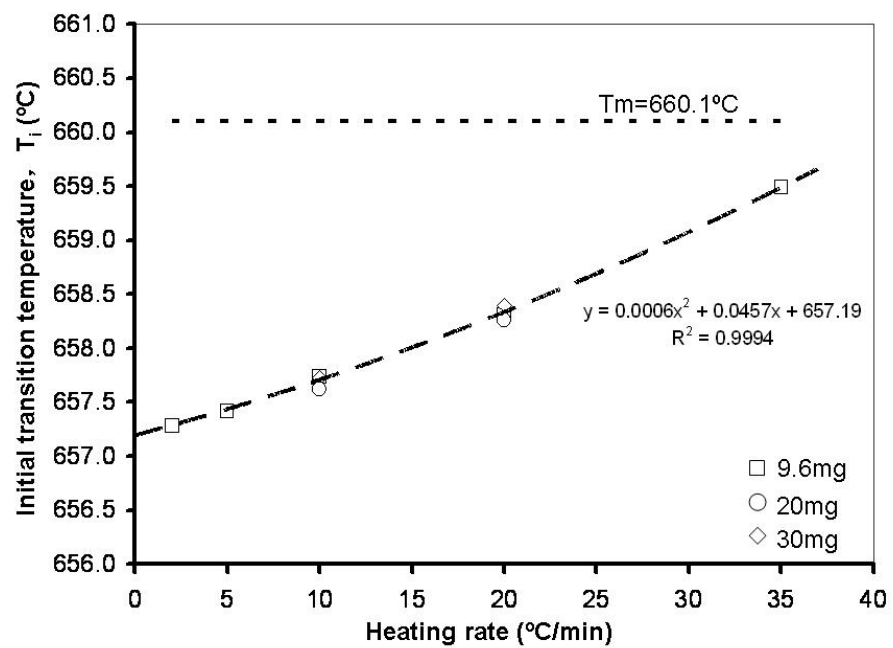


Figure 4-7 Combination of the heating rate and mass effect on  $T_i$  of aluminum pellet samples (uncorrected data)

#### **4.1.4. Effect of sample geometry on phase transition temperature**

Four types of aluminum samples were used to study the effect of sample geometry on the phase transition temperature, namely three powders with mean diameters of: 37 $\mu\text{m}$ , 112 $\mu\text{m}$ , and 1500 $\mu\text{m}$ , and one thin disc pellet with a diameter of 4100 $\mu\text{m}$ . Sample masses of 9.6mg, 20mg and 30mg were investigated for each type of geometry.

The raw results were plotted for each mass to compare the geometry effect (Figure 4-8). The sharp peak for the pellet sample clearly distinguishes it from the shallow peaks of the powder samples for every mass group. The shallow and smooth peaks obtained for the powder samples are likely to be caused by the loose packing of the powders and poor heat diffusion through the powder samples.

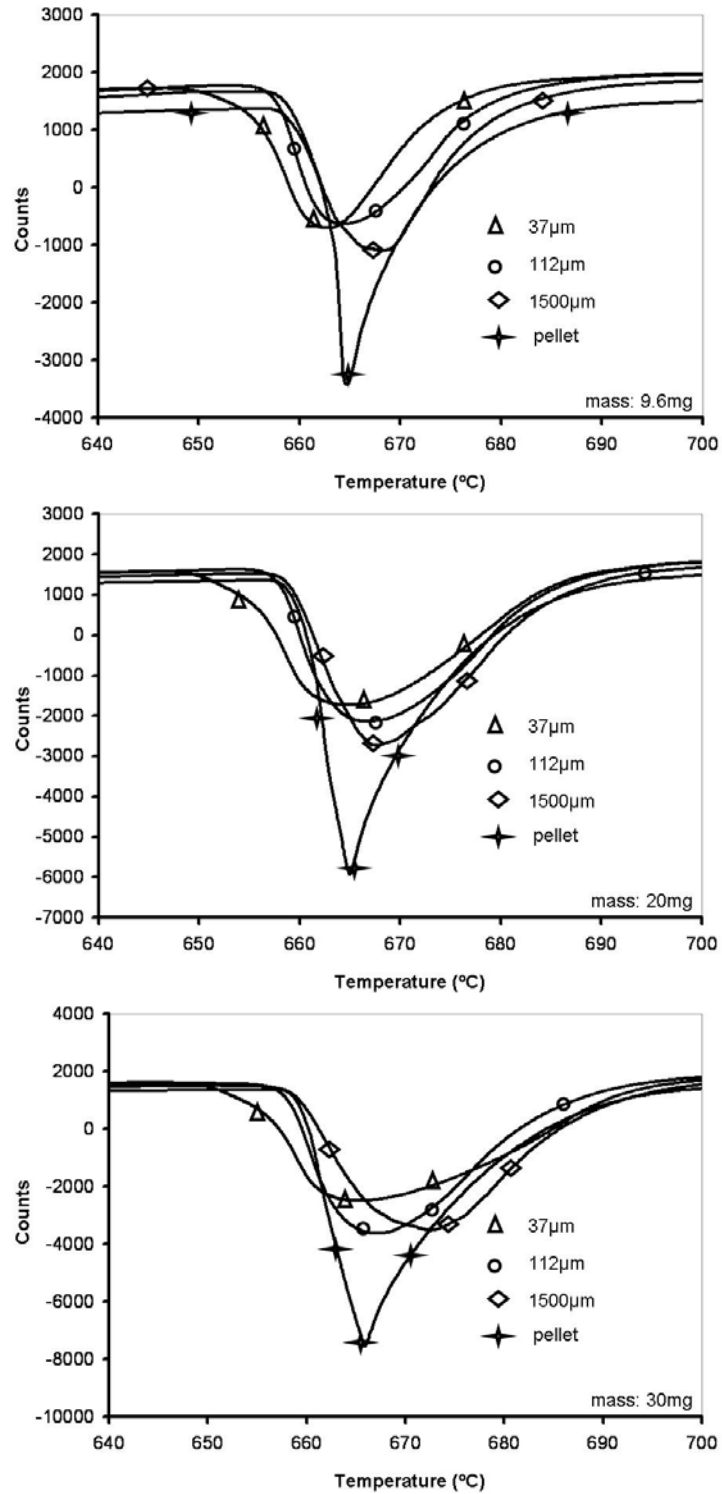


Figure 4-8 Raw results of geometry effect on  $T_i$  for aluminum samples with masses: 9.6mg, 20mg and 30mg

The initial transition temperatures for the various mean particle sizes and sample mass sizes are listed in Table 4-4. The maximum standard deviation of initial transition temperature among the various mass, same geometry samples is less than 0.026, in agreement with the previous result that the mass effect is insignificant compared with the heating rate and sample geometry.

Table 4-4 Initial transition temperature for various mean particle sizes

	Initial transition temperature (°C)				Standard derivation
	9.6mg	20mg	30mg	Average	
<b>37µm</b>	648.58	648.56	648.57	648.57	0.01
<b>112 µm</b>	655.83	655.82	655.80	655.82	0.01528
<b>1500 µm</b>	657.28	657.24	657.25	657.26	0.02082
<b>4100 µm</b>	658.31	658.29	658.34	658.31	0.02516



It should be noted, however, that there is a distinguishable initial phase transition temperature difference between different geometry samples. Figure 4-9 shows that the initial transition temperature decreases as the mean particle size decreases. From a thermodynamics point of view, the greater surface energy contributes to the phase transition free energy as the particle size decreases since the total surface area of the sample increases significantly as the particle size decreases (Hasegawa *et al.*, 1980). The relationship between the initial phase transition temperature and the sample geometry was plotted as a function of the reciprocal of the sample mean particle radius and the results are shown in Figure 4-10, where the pellet sample is assumed to be a particle with 4100 $\mu\text{m}$  diameter. This result is in agreement with previous work concerning the size dependence of the melting temperature in metals (Buffat and Borel, 1976; Couchman and Jesser, 1977; Allen *et al.*, 1986; Lai *et al.*, 1996; Guisbiers and Wautelet, 2006).

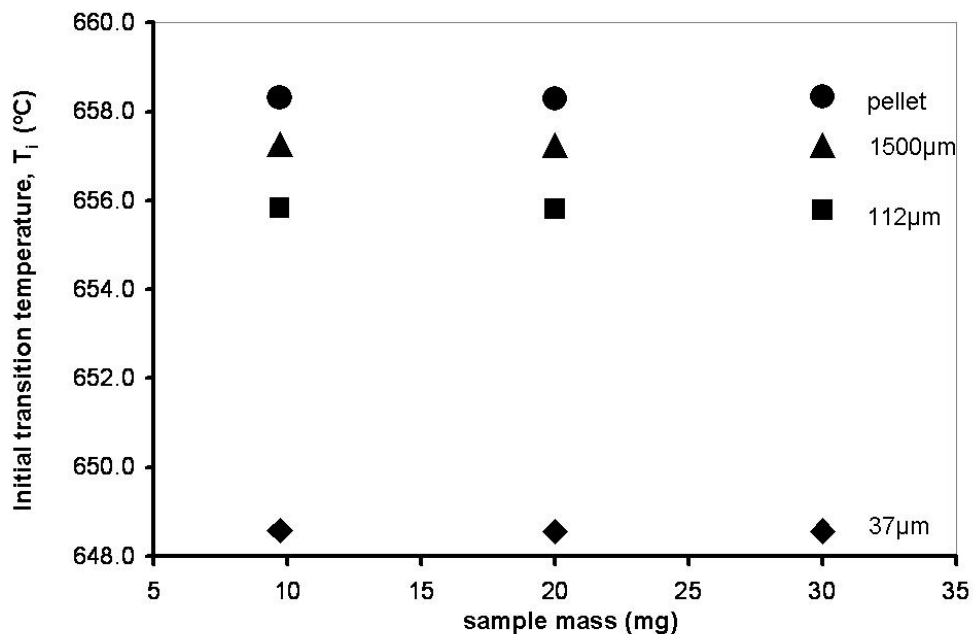


Figure 4-9 Effect of mass and particle size on  $T_i$  of aluminum samples

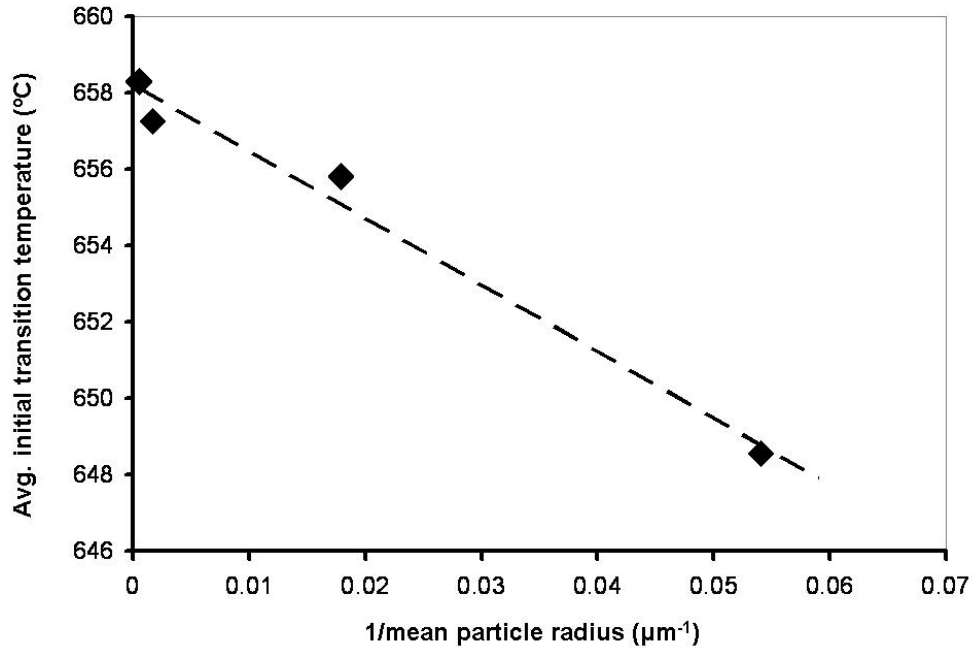


Figure 4-10 Effect of aluminum particle size on the initial phase transition temperature

## 4.2. Transition heat measurements

### 4.2.1. Sensitivity calibration

Sensitivity calibration is a fundamental step in heat-flux type DSC measurements. Measuring a standard sample with known heat capacity makes it possible to convert the raw electrical signal into the heat flow involved in the thermal process, making quantification possible for enthalpy calculations. Generally it involves two steps: the net standard sample measurement and the sensitivity calculation by the instrument's built-in software. The net standard sample measurement requires the measurements of the zeroline (empty crucible) and the standard sample to be acquired separately. The purpose of this two-step measurement is to eliminate the signal due to the thermal capacitance

from the sample container (crucible). Here, the effect of the heating rate on the sensitivity calibration was studied using the net results of the standard sapphire disc, as shown in Figure 4-11, and the sensitivity calibration curve, shown in Figure 4-12.

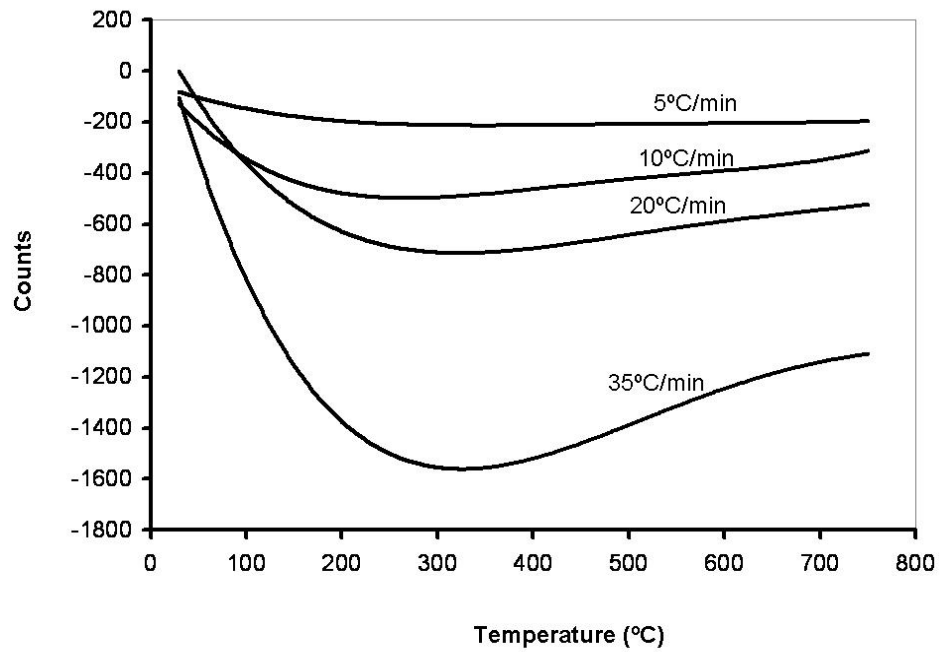


Figure 4-11 The net results for the standard sapphire disc at various heating rates

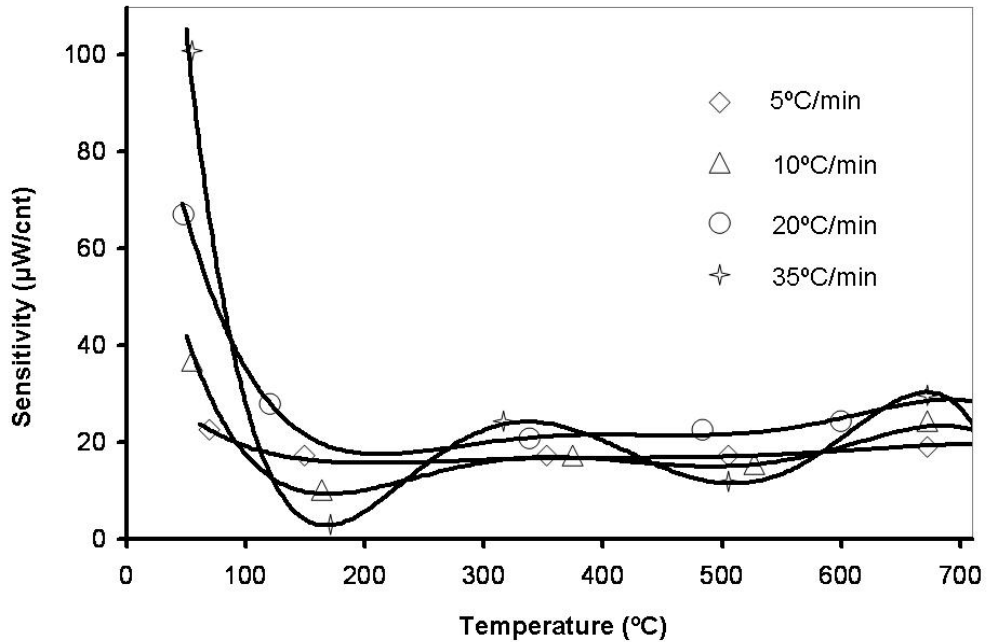


Figure 4-12 Sensitivity calibration at various heating rates

Comparing the sensitivity calibration curves, higher heating rates produce larger temperature gradients. The raw results represent the electrical potential due to the temperature difference between the sample and the reference. So the absolute value of the raw signal increases with increasing heating rate in Figure 4-11. The sensitivity calibration results failed to show a similar trend to that observed for the previously reported heating rate effect. From the sensitivity calibration data of Figure 4-12, the most constant sensitivity calibration curve appears to be at a heating rate of 5°C/min.

#### 4.2.2. Phase transition enthalpy measurements

The effect of various experimental factors on the phase transition enthalpy was studied through their effect on the heat calibration factor for high purity aluminum. Three powders and one pellet aluminum samples were measured at heating rates of 10°C/min and 20°C/min for three mass sizes 9.6mg, 20mg and 30mg. The results are listed in Table 4-4.

In Table 4-4, the total surface area of the samples was evaluated by two methods depending on the sample type: 1) the three types of powder are assumed to be ideal spheres, and the mean particle size represents every particle; and 2) the pellet sample is assumed to be an ideal cylinder. Hence, the total surface area was calculated as follows:

1) for spherical powders

According to the above assumptions, the total surface area of the powder is equal to the product of the total number of particles ( $n$ ) and the surface area of a single particle ( $A_1$ ):

$$A_{total} = n * A_1 \quad (4-1)$$

The total number of particle can be calculated from the total sample mass ( $m$ , mg) and the single particle mass ( $m_1$ ):

$$n = \frac{m}{m_1} = \frac{m}{\rho * V_1} = \frac{m}{\rho * \frac{4}{3} \pi * r^3} \quad (4-2)$$

$$\text{The surface area of a single particle is: } A_1 = 4 * \pi * r^2 \quad (4-3)$$

Substituting Equations (4-2) and (4-3) into Equation (4-1), the total surface of the sample is:

$$A_{total} = \frac{30 * m^2}{\rho * r} \quad (4-4)$$

Here,  $\rho$  is the density of the sample ( $\text{g}/\text{cm}^3$ ) and  $r$  is the mean radius of each type of powder ( $\mu\text{m}$ )

2) for cylindrical pellets

The total surface area of the cylinder can be calculated as:

$$A = (2\pi r^2 + 2\pi r h) * 10^{-8} \quad (4-5)$$

Where  $h$  is the sample thickness ( $\mu\text{m}$ )

The measured transition heat (i.e. the heat flow peak area in time scale plot) decreases with increasing sample mass and decreasing particle size and heating rates in Table 4-5. From observations of measured samples, the samples lost luster on their surface, which indicated that samples were oxidized during the measuring processes. Since the exothermic oxidation process “interferes” with the endothermic melting process, sample oxidation will reduce the measured transition heat. Here, slower heating rates and finer particle sizes could enhance the oxidation effect and, as a consequence, reduce the measured transition heats. The detailed effects from these experimental factors will be discussed in the following sections.

Table 4-5 Measured transition heat of aluminum under each measuring condition

Mean particle size ( $\mu\text{m}$ )	Mass (mg)	Total surface area ( $\text{cm}^2$ )	10°C/min		20°C/min	
			Measured fusion heat (J/g)	Heat calibration factor, $K_Q$ ( $\text{mg}^{-1}$ )	Measured fusion heat (J/g)	Heat calibration factor, $K_Q$ ( $\text{mg}^{-1}$ )
37	9.6	5.8258	255.55	1.5496	313.796	1.2620
	20.0	12.0119	260.185	1.5220	311.35	1.2719
	30.0	18.0178	257.2	1.5397	303.2375	1.3059
112	9.6	1.9246	-	-	315.953	1.2534
	20.0	3.9682	-	-	313.7233	1.2623
	30.0	5.9523	-	-	304.0159	1.3026
1500	9.6	0.1796	-	-	345.0079	1.1478
	20.0	0.3704	-	-	333.7006	1.1867
	30.0	0.5556	-	-	328.0745	1.2070
pellet	9.6	0.2871	305.51	1.2962	402.9283	0.9828
	20.0	0.3253	308.50	1.2836	392.9554	1.0077
	30.0	0.3623	309.57	1.2792	383.962	1.0314

#### 4.2.2.1. Effect of heating rate on phase transition heat measurements

The fine powder (37 $\mu$ m) and pellet aluminum samples were studied at heating rates of 10°C/min and 20°C/min to determine the effect of heating rate on the heat calibration factor. Recall from section 3.2.4 that the heat calibration factor is defined as:

$$K_Q = \frac{Q_{true, std}}{A_{std}}$$

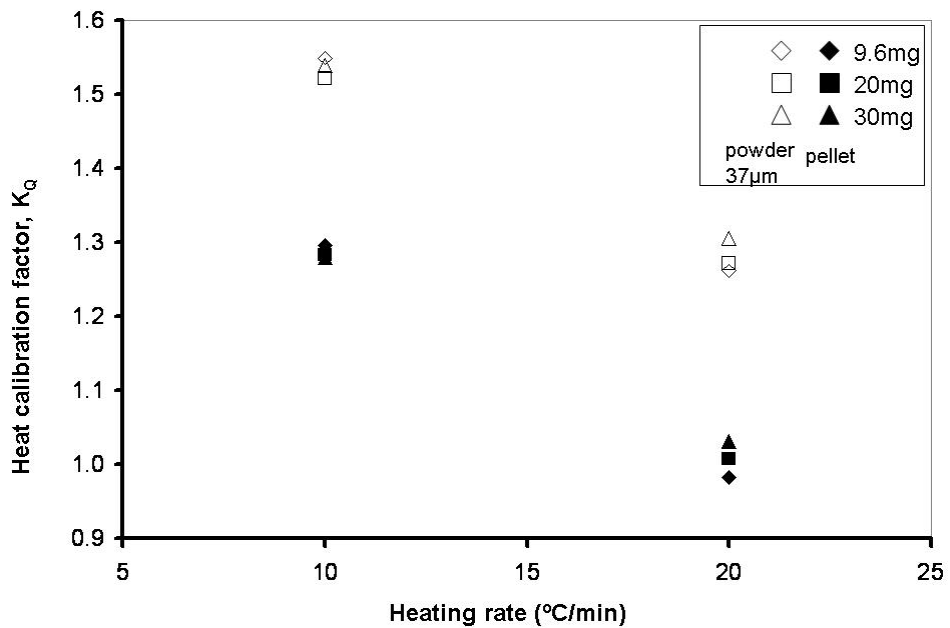


Figure 4-13 Effect of heating rate on heat calibration factor for aluminum pellet and powder

The results showed that the heat calibration factor decreased with increasing heating rate for both the powder and pellet for of aluminum (Figure 4-13). This result disagrees with the results reported by the GEFTA group, who found that the heat



calibration factor slightly increased with the heating rate, but this variation occurred only for a small range of  $K_Q$  around 1 (Gmelin and Sarge, 1995). This conflicting result may be explained by the aluminum oxidation that affected the samples in these measurements. As explained in section 3.3, the melting process and the oxidation reaction are two opposing thermal phenomena; the first being endothermic and the second exothermic. Oxidation of the sample will reduce the melting peak area, thus increasing the heat calibration factor. Here, the higher heating rate leads to a shorter phase transition interval, reducing the oxidation effect. Therefore, here the heat calibration factor decreased with increasing heating rate. However, since there is insufficient information provided in GEFTA's document, it was not possible to analyze the reasons behind their results. Moreover, the heat calibration factor for pellet samples at 20°C/min was observed to be closer to 1 than that of the powder samples.

Besides the heating rate, the geometric form of the samples also has a significant effect on the heat calibration factor (Figure 4-13). The heat calibration factor of powder samples is much greater than for the pellet form. It seems likely that the oxidation contribution to the heat calibration factor also applies here. In general, the powder samples have a greater total surface area than the pellet samples. Thus, the phase transition peak area will be significantly reduced for oxidizing powder samples compared with the pellet samples. As a consequence, a greater heat calibration factor is observed for the powder samples.

#### **4.2.2.2. Effect of sample mass and geometry on phase transition enthalpy measurements**

The effect of sample mass on the heat calibration factor was studied at a heating rate of 20°C/min for four geometric types of aluminum samples. The plot of the heat calibration factor as a function of sample mass (Figure 4-14) revealed that a slight increase in the heat calibration factor occurred with increasing sample mass, and the heat calibration factor of a pellet sample was closer to 1 compared with the powder sample. These observations match results reported from Gmelin's group (Gmelin and Sarge, 1995). Here, as the sample mass increases, the total surface area of the sample also increases. Thus, oxidation of the sample reduces the peak area of the phase transition, and as result, the heat calibration factor increases with sample mass size.

The pellet samples have fewer oxidation effects due to their smaller total surface area comparing with powder samples with the same mass, thus their heat calibration factor is close to 1, which means that oxidation effects are minimal and the measured phase transition enthalpy is close to its true value.

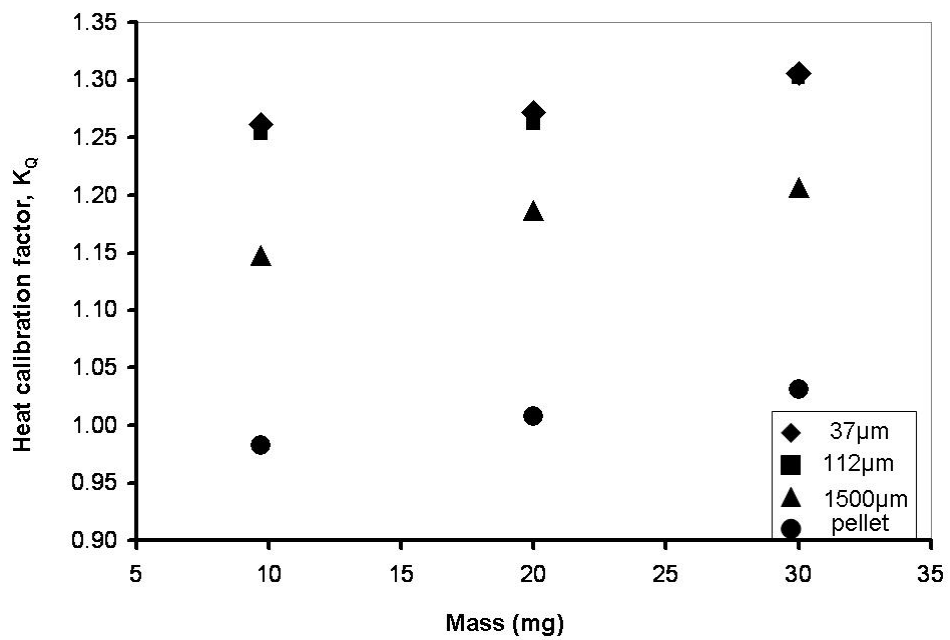


Figure 4-14 Effect of sample mass size and geometry on the heat calibration factor for various aluminum samples

#### 4.2.2.3. Relationship between heat calibration factor and total surface area

Since the degree of oxidation depends on the total surface area of the sample, the relationship between the heat calibration factor and the total surface area of sample was studied. The plot of the heat calibration factor as a function of the total surface area of the sample (Figure 4-15) reveals that the curve can be divided into two stages, an initial sharp increase of the heat calibration factor followed by a gradual increase at greater total surface area.

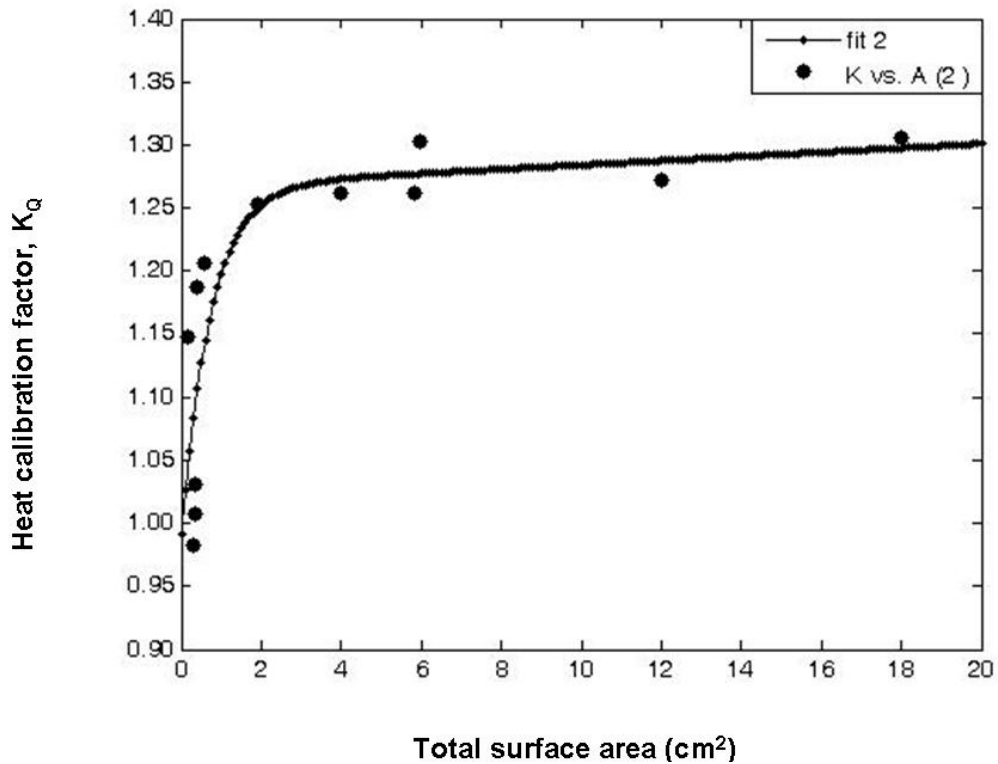


Figure 4-15 Relationship of heat calibration factor and total surface area of aluminum

### **4.3. Calculation of the oxidation effect on $C_p$ measurement**

#### **4.3.1. The effect of the presence of aluminum oxide on $C_p$ measurements**

The change in the total mass during the measurement can be found from the TGA measurement results (Figure 4-16). All four geometries samples increased their total mass as the temperature increased. For the pellet and coarse powder samples, this change occurred gradually and slowly, while for the two finer powders, the total mass increased slowly at lower temperatures but rapidly at temperatures above 400°C. This observation can once again be explained by the oxidation involved in the measuring process (Eisenreich et al., 2004; Trunov et al., 2006). Here, the marked difference in the total surface area between pellets and fine powders likely contributes to the results shown in Figure 4-16.

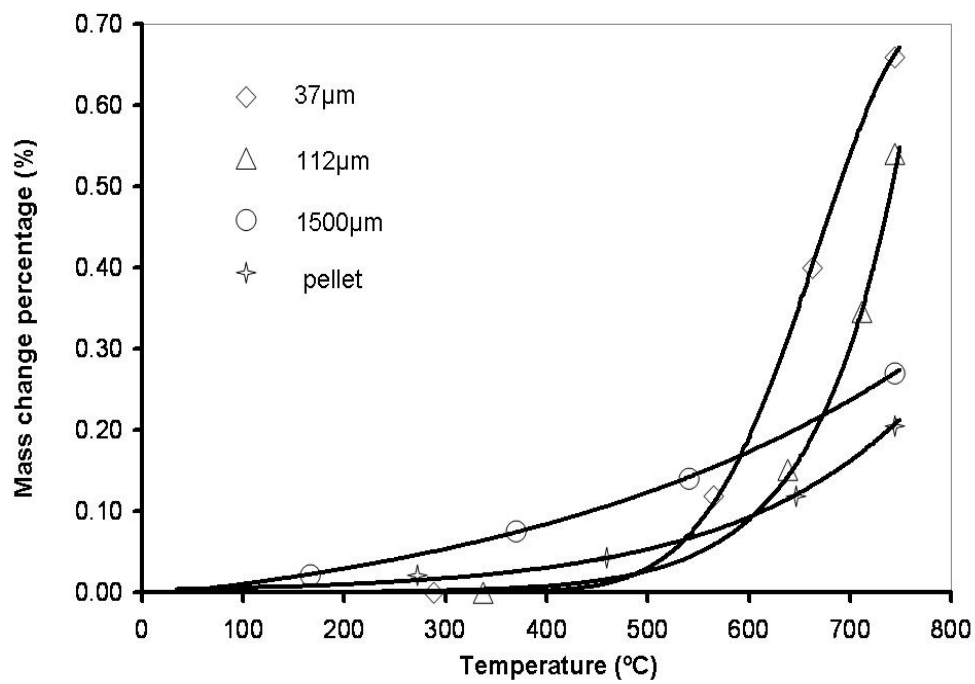


Figure 4-16 The mass change of 20mg aluminum samples with various sample geometries

The effect due to the amount of aluminum oxide generated was compared only between the two extreme cases: pellets and the 37 $\mu$ m powder. The amount of aluminum oxide can be calculated from the total mass change given by the TGA results based on the mass conservation law during the chemical reaction. Figure 4-17 shows the change in the mass of the aluminum oxide for both the pellet and powder37 samples for samples with an initial mass of 20mg of aluminum.

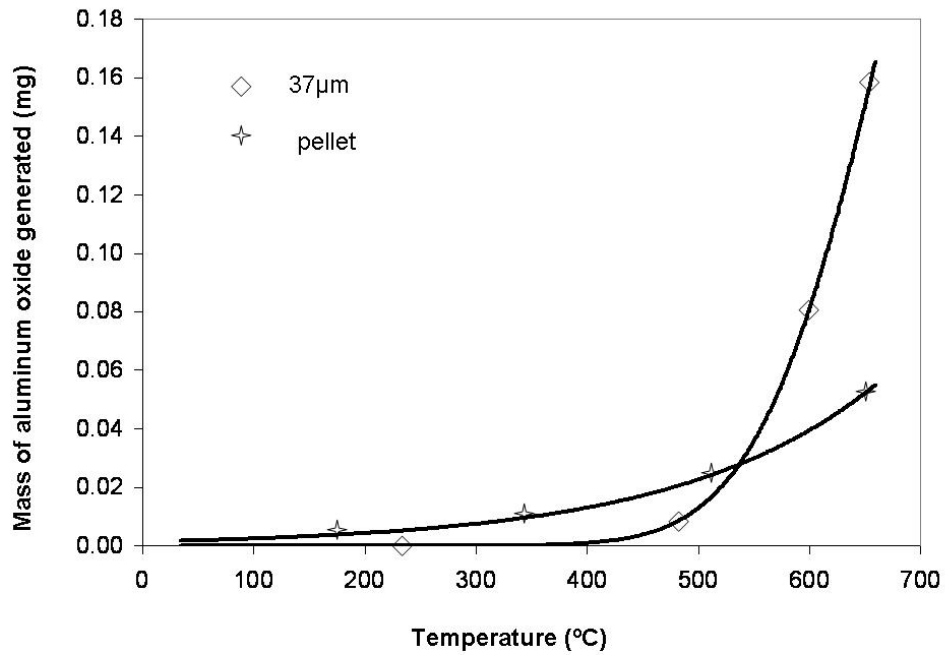


Figure 4-17 Aluminum oxide generated from aluminum with an initial sample mass of 20mg

Finally the effect of the amount of the aluminum oxide on  $C_p$  measurements can be calculated and is plotted in Figure 4-18. The deviation on the true specific heat capacity due to the presence of aluminum oxide from the heating process is less than 0.01% (Figure 4.18), in other words, the effect of the alumina surface films on the heat capacity measurements can be neglected.

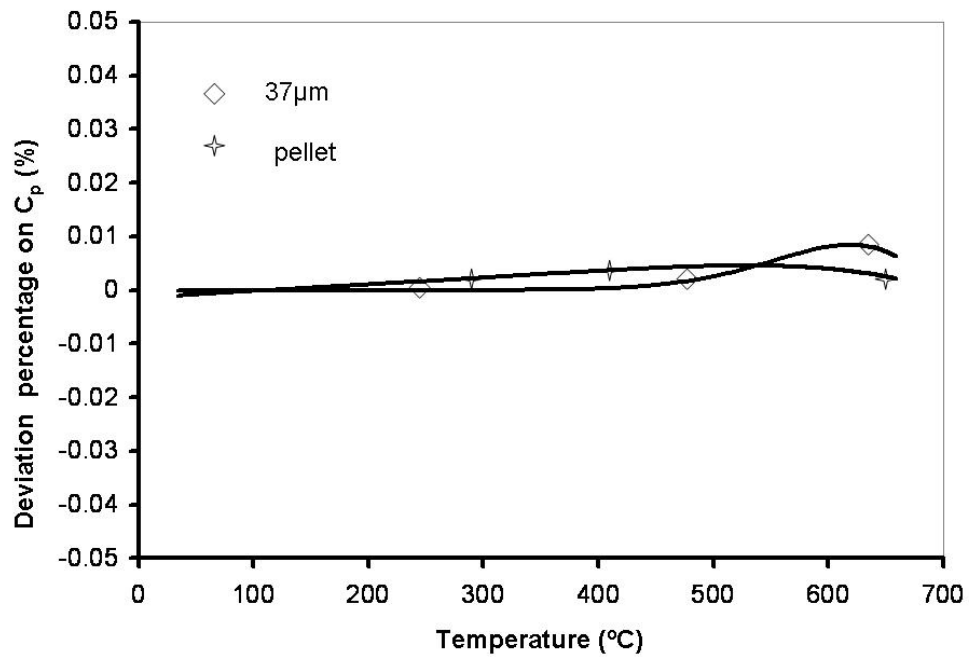


Figure 4-18 Change in  $C_p$  due to the presence of alumina surface film



### **4.3.2. Effect of the oxidation reaction enthalpy on $C_p$ measurements**

Calculating the effect due to the reaction enthalpy of the aluminum oxidation consists of three steps: i) calculating the reaction enthalpy; ii) calculating the mass rate of the aluminum oxide generation; iii) converting the reaction enthalpy into the heat flow. The calculation results of relative properties are summarized in Table 4-6 and the results of the three steps are shown in Figure 4-19. Figure 4-19 reveals that even though the reaction enthalpy slightly decreased with increasing temperature, the positive change in the mass rate vs. temperature made the overall heat flow from the oxidation reaction increase as the temperature increased.

Table 4-6 Calculation results for the oxidation reaction heat flow

Temperature (°C)	Reaction heat (J/g) (dH/dm)	Mass rate (mg/s) (dm/dt)		Equivalent reaction heat flow (mW) (dH/dt)	
		powder37	pellet	powder37	pellet
40	16443.13	3.61E-07	1.10E-06	5.93E-03	1.81E-02
60	16459.71	-3.98E-07	2.22E-06	-6.54E-03	3.65E-02
80	16477.04	1.18E-07	3.06E-06	1.93E-03	5.02E-02
100	16495.02	3.11E-07	3.90E-06	5.12E-03	6.41E-02
120	16513.57	2.26E-07	4.78E-06	3.72E-03	7.86E-02
140	16532.61	2.48E-08	5.71E-06	4.08E-04	9.38E-02
160	16552.10	-1.65E-07	6.68E-06	-2.71E-03	1.10E-01
180	16571.98	-2.66E-07	7.71E-06	-4.37E-03	1.27E-01
200	16592.21	-2.51E-07	8.80E-06	-4.13E-03	1.45E-01
220	16612.77	-1.31E-07	9.98E-06	-2.15E-03	1.64E-01
240	16633.63	6.06E-08	1.13E-05	9.95E-04	1.85E-01
260	16654.75	2.82E-07	1.26E-05	4.62E-03	2.07E-01
280	16676.13	5.05E-07	1.41E-05	8.29E-03	2.32E-01
300	16697.73	7.46E-07	1.58E-05	1.23E-02	2.59E-01
320	16719.56	1.09E-06	1.76E-05	1.79E-02	2.89E-01
340	16741.59	1.75E-06	1.96E-05	2.87E-02	3.21E-01
360	16763.80	3.05E-06	2.18E-05	5.01E-02	3.57E-01
380	16786.20	5.56E-06	2.42E-05	9.11E-02	3.96E-01
500	16808.76	1.00E-05	2.68E-05	1.64E-01	4.40E-01
420	16831.48	1.74E-05	2.97E-05	2.86E-01	4.87E-01
440	16854.35	2.90E-05	3.29E-05	4.76E-01	5.40E-01
460	16877.37	4.62E-05	3.65E-05	7.58E-01	5.98E-01
480	16900.53	7.06E-05	4.04E-05	1.16E+00	6.63E-01
500	16923.81	1.04E-04	4.49E-05	1.70E+00	7.35E-01
520	16947.22	1.47E-04	4.98E-05	2.40E+00	8.16E-01
540	16970.75	2.00E-04	5.53E-05	3.28E+00	9.06E-01
560	16994.40	2.63E-04	6.15E-05	4.31E+00	1.01E+00
580	17018.15	3.33E-04	6.84E-05	5.46E+00	1.12E+00
600	17042.02	4.05E-04	7.60E-05	6.64E+00	1.25E+00
620	17065.98	4.71E-04	8.43E-05	7.72E+00	1.38E+00
640	17090.04	5.16E-04	9.34E-05	8.47E+00	1.53E+00

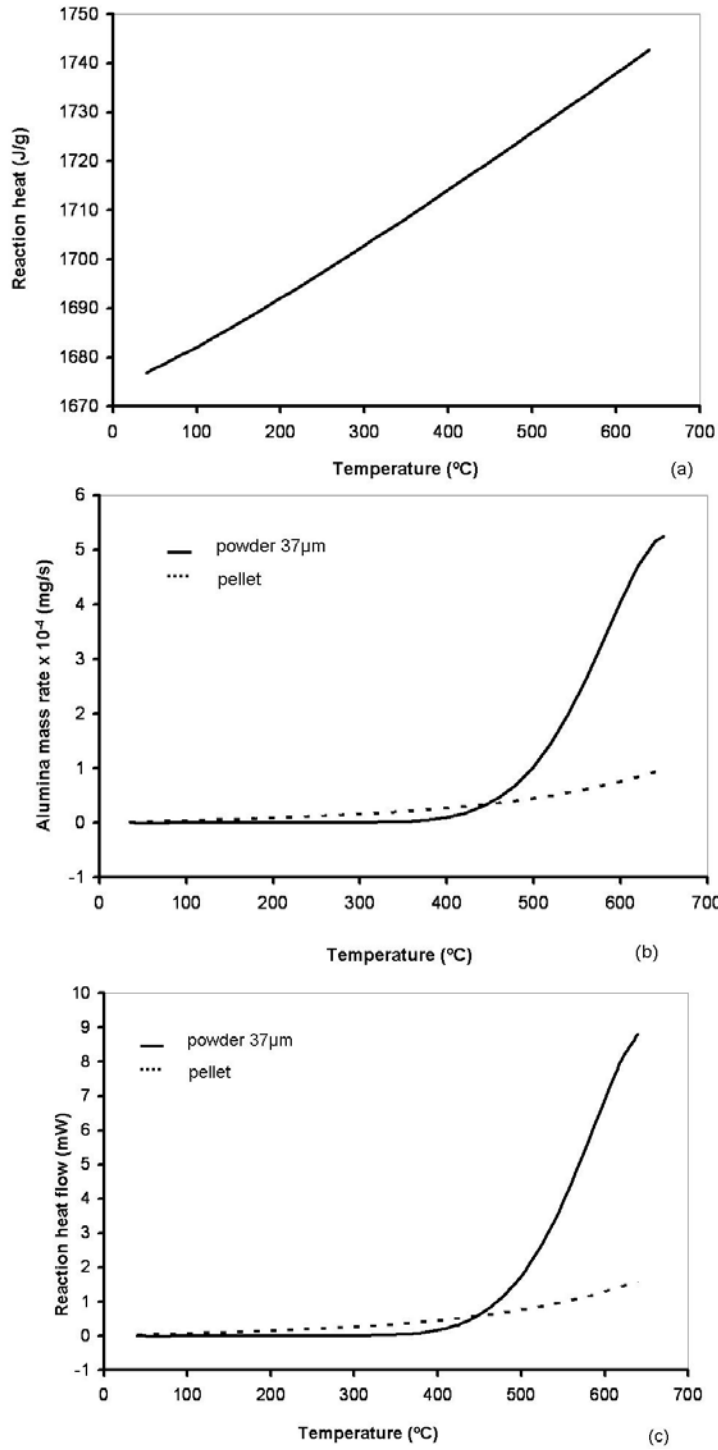


Figure 4-19 Effects of oxidation reaction for 20mg aluminum: powder37 and pellet  
 (a) reaction enthalpy; (b) mass rate of aluminum oxide generated;  
 (c) converted heat flow from reaction enthalpy

In order to evaluate the change in the  $C_p$  measurement due to the oxidation reaction enthalpy, the true heat flow of the sample was calculated according to Equation 3-6 from the true  $C_p$  of aluminum, and the measured heat flow to the standard sapphire and zeroline. The results are shown in Figure 4-20.

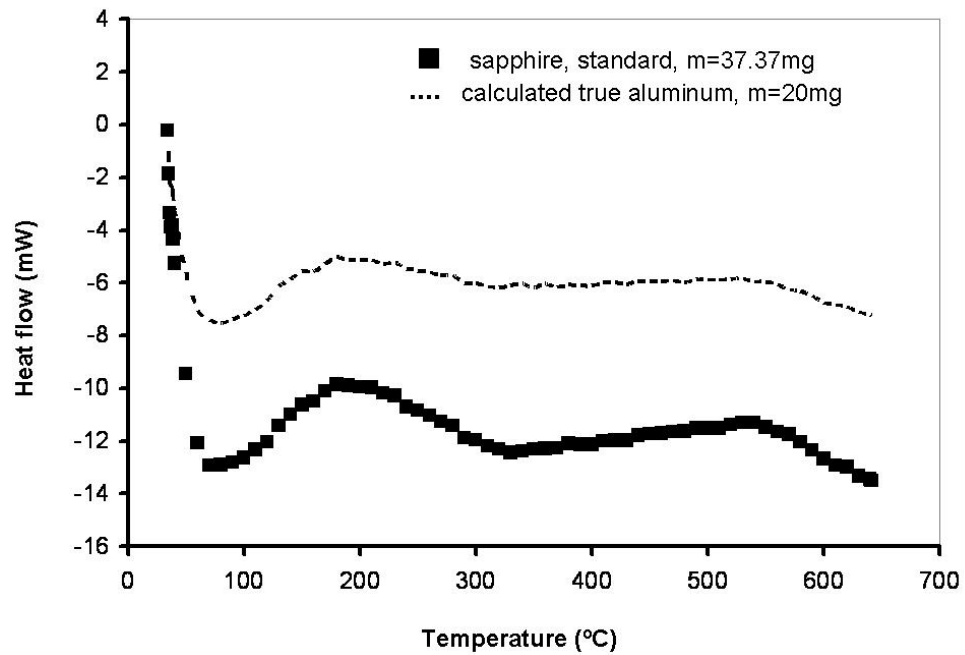


Figure 4-20 Measured heat flow of standard sapphire and calculated true heat flow for aluminum

The heat flow of aluminum sample can be corrected by subtracting the oxidation reaction from the original heat flow signal. Figure 4-21 gives the corrected measurement results for aluminum samples. Although the corrected results are not ideal using the oxidation enthalpy method, they do show that the oxidation reaction enthalpy can contribute to inaccuracy of in such measurements. It is therefore recommended that steps should be taken to avoid sample oxidation in order to obtain accurate  $C_p$  measurements.

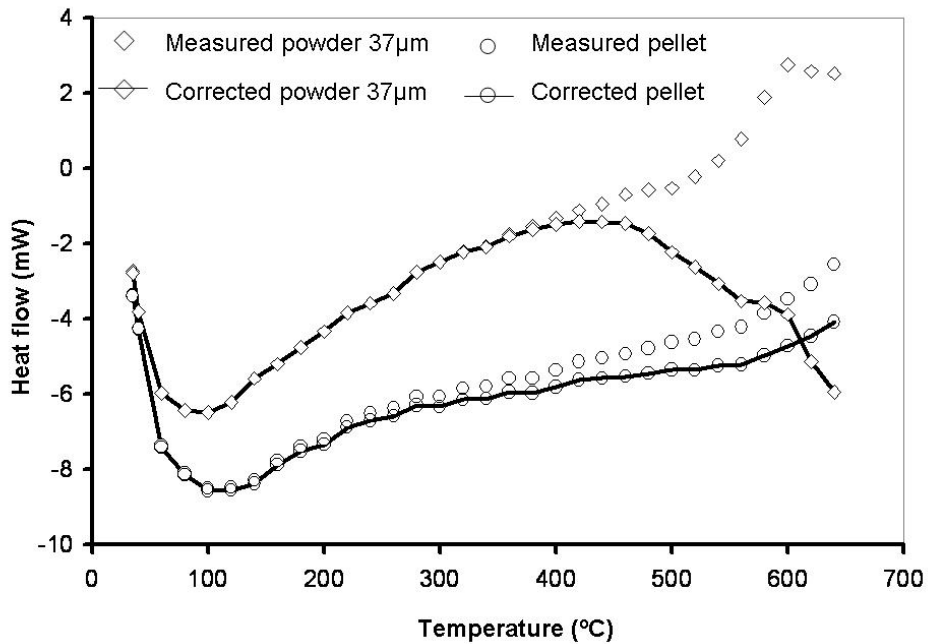


Figure 4-21 The corrected heat flow of aluminum powder and pellet samples by oxidation reaction enthalpy

The deviation due to the oxidation reaction on the heat capacity measurements can be easily found using the ratio of the converted heat flow from the reaction enthalpy and the true heat flow of the samples, as illustrated in Figure 4-22. The influence of the reaction heat of the fine powder sample increases dramatically, especially above 400°C.

Unlike the powder samples, however, the effect in the pellet sample only gradually increases as the temperature increases.

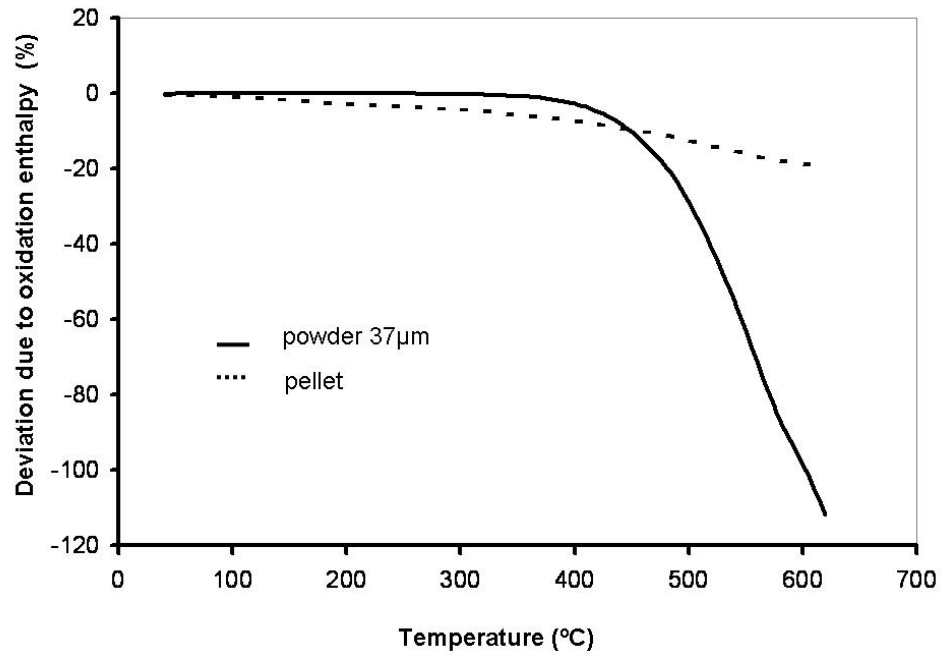


Figure 4-22 Deviation in  $C_p$  measurement due to the oxidation reaction

## 5. CONCLUSIONS

For general quantitative phase transition temperature determination, a higher heating rate and larger sample mass make the phase transition peak easier to observe; however, this may not be appropriate for materials exhibiting phase transitions in close proximity on the temperature scale.

The initial phase transition (i.e., melting) temperature decreases with increasing heating rates and decreasing particle size. The effect of overall sample mass is insignificant. A temperature correction curve for the combined effect of heating rate and sample mass was determined.

Compared with the effect from the oxidation reaction enthalpy, the effect of the simple presence of oxide in heating process on specific heat capacity ( $C_p$ ) measurements was insignificant. On the other hand, the oxidation reaction enthalpy has a significant deviation on specific heat capacity ( $C_p$ ) measurements above 400°C.

The heat calibration factor increases with decreasing heating rates, in disagreement with some literature results. However, this discrepancy can be explained by sample oxidation involved in the measuring process. The heat calibration factor also increases with increases in the total surface area of samples in agreement with the oxidation effect on the phase transition heat.

## **6. SUGGESTIONS FOR FUTURE RESEARCH**

Additional experiments are needed to further improve the operational procedures of differential scanning calorimetry.

An effective way to avoid the effects of oxidation during differential scanning calorimetry needs to be developed. Perhaps small Titanium chips can be placed in the furnace to getter the oxygen present.

To improve the measuring accuracy of STA1500, the other experimental factors, the effects of the flow rate of the environment gas on these measurements requires further study.



## REFERENCES

- Allen, G. L., Bayles, R. A., Gile, W. W. and Jesser, W. A. (1986). "Small particle melting of pure metals." Thin solid films **144**: 297-308.
- ASTM-E967-97 (2000). "Differential scanning calorimeters and differential thermal analyzers." ASTM **14.02**.
- ASTM-E968-99 (2000). "Standard practice for heat flow calibration of differential scanning calorimeters." ASTM **14.02**.
- Barrall, E. M. (1973). "Precise determination of melting and boiling points by differential thermal analysis and differential scanning calorimetry." Thermochimica Acta **5**(4): 377-389.
- Bortfeldt, J. and Kramer, B. (1991). Units in physics and chemistry, Springer.
- Brandts, J. F. and Lin, L. N. (1990). "Study of strong to ultratight protein interactions using differential scanning calorimetry." Biochemistry **29**(6927-6940).
- Breuer, K. H. and Eysel, W. (1982). "The calorimetric calibration of differential scanning calorimetry cells." Thermochimica Acta **57**: 317-329.
- Buffat, P. and Borel, J.-P. (1976). "size effect on the melting temperature of gold particles." Phys. Rev. A **13**(6): 2287-2298.

- Callanan, J. E., Mcdermott, K. M., Weir, R. D. and Westrum, E. F. (1992). "Comparison of heat capacities measured by adiabatic calorimetry and by scanning calorimetry: thermodynamic properties of 9-methylcarbazole at temperatures between 4 K and 345 K." The Journal of Chemical Thermodynamics **24**(3): 233-243.
- Callanan, J. E. and Sullivan, S. A. (1986). "Development of standard operating procedures for differential scanning calorimeters." Rev. Sci. Instrum. **57**(10): 2584-2592.
- Cammenga, H. K., Eysel, W., Gmelin, E., Hemminger, W., Höhne, G. W. H. and Sarge, S. M. (1993). "The temperature calibration of scanning calorimeters part 2. calibration substances." Thermochimica Acta **219**: 333-342.
- Cao, W. D., Kennedy, R. L. and Willis, M. P. (1991). Superalloys 718, 625 and various derivatives. TMS, Warrendale, PA.
- Castro, C. A. N. d., Lourenco, M. J. V. and Sampaio, M. O. (2000). "Calibration of a DSC: its importance for the traceability and uncertainty of thermal measurements." Thermochimica Acta **347**: 85-91.
- Chase, M. W. J. (1998). "NIST-JANAF Thermodynamical Table." J. Phys. Chem. Ref. Data Monograph **9**: 1-1951.
- Cieslak, M. J., Headley, T. J., Knorovsky, G. A., Roming, A. D. and Kollie, T. (1990). "A comparison of the solidification behavior of Incoloy 909 and inconel 718." Metall. Trans. A **21A**: 479-488.
- Couchman, P. R. and Jesser, W. A. (1977). ""Thermodynamic theory of size dependence of melting temperature in metals"." Nature **269**: 481-483.

- Cox, J. D., Wagman, D. D. and Medvedev, V. A. (1984). CODATA Key Values for thermodynamics. New York, Hemisphere Publishing Corp.
- Dong, H. B. and Hunt, J. D. (2000). A numerical model of two-pan heat flux DSC, which allows accurate results to be calculated from experiment. The 14th symposium on thermophysical properties.
- Eisenreich, N., Fietzek, H., Juez-Lorenzo, M. d. M., Kolarik, V., Koleczko, A. and Weiser, V. (2004). "On the mechanism of low temperature oxidation for aluminum particles down to the nano-scale." Propellants, explosives, pyrotechnics **29**(3): 137-145.
- Fasoyinu, Y., Barry, J., Sahoo, M., Labelle, P., Wang, D. and Overfelt, R. A. (2003). "Thermophysical properties of magnesium alloys AE42, AJ52X and AM60B." AFS Transactions **111**: 1031-1052.
- Freire, E., Osdol, W. W., Mayorga, O. L. and Sanchez-Ruiz, J. M. (1990). "Calorimetrically determined dynamics of complex unfolding transitions in proteins." Annual Reviews of Biophysics and Biophysical Chemistry **19**: 159-188.
- Gaskell, D. R. (1995). Introduction to the thermodynamics of materials. Washington, D.C, Taylor & Francis.
- Gatta, G. D., Richardson, M., Sarge, S. M. and Stölen, S. (2006). "Standards, calibration, and guidelines in microcalorimetry part2. calibration standards for differential scanning calorimetry IUPAC Technical Report." Pure & Appl. Chem. **78**(7): 1455-1476.
- Gmelin, E. and Sarge, S. M. (1995). "Calibration of differential scanning calorimeters." Pure & Appl. Chem. **67**(11): 1789-1800.

- Gmelin, E. and Sarge, S. M. (2000). "Temperature, heat and heat flow rate calibration of differential scanning calorimeters". Thermochemica Acta **347**: 9-13.
- Guisbiers, G. and Wautelet, M. (2006). "size, shape and stress effects on the melting temperature of nanopolyhedral grains on a substrate." Nanotechnology **17**: 2008-2011.
- Hakvoort, G., Hol, C. M. and Ekeren, P. J. v. (2001). "DSC calibration during cooling: a survey of possible compounds." Journal of Thermal Analysis and Calorimetry **64**: 367-375.
- Hasegawa, M., Hoshino, K. and Watabe, M. (1980). "A theory of melting in metallic small particles." Journal Physics F: Metal Physics **10**: 619-635.
- Höhne, G. W. H. (1983). "Problems with calibration of differential-temperature-scanning-calorimeters." Thermochemica Acta **69**(175-197).
- Höhne, G. W. H., Cammenga, H. K., Gmelin, E., Eysel, W. and Hemminger, W. (1990). "The temperature calibration of scanning calorimeters." Thermochemica Acta **160**: 1-12.
- Höhne, G. W. H., Hemminger, W. F. and Flammersheim, H. J. (2003). Differential Scanning Calorimetry, Springer.
- Holubova, J., Cernosek, Z. and Cernoskova, E. (2000). "Kinetic analysis of non-isothermal DSC data: computer-aided test of its applicability." Journal of Thermal Analysis and Calorimetry **62**: 715-719.
- Jacob, S. and Schlesinger, M. E. (2006). "Evaluation of the accuracy and reproducibility of a high-temperature differential scanning calorimeter by heat capacity measurements." American Laboratory **38**(14): 13-15.

- Jacob, S. and Schlesinger, M. E. (2006). A study of accuracy and reproducibility of high temperature differential scanning calorimetry. TMS Annual meeting, EPD Congress: 209-217.
- Kalantary, M. R., Conway, P. P., Sarvar, F. and Williams, D. J. (1995). "Towards a standard for differential scanning calorimetry." IEEE/CPMT Int'l electronics manufacturing technology symposium: 337-343.
- Lai, S. L., Guo, J. Y., Petrova, V., Ramanath, G. and Allen, L. H. (1996). "Size-dependent melting properties of small tin particles: nanocalorimetric measurements." Phys. Rev. Lett. **77**: 9-102.
- Martins, J. A. and Cruz-Pinto, J. J. C. (1999). "The temperature calibration on cooling of differential scanning calorimeters." Thermochimica Acta **332**: 179-188.
- Mraw, S. C. and Naas, D. F. (1979). "The measurement of accurate heat capacities by differential scanning calorimetry comparison of d.s.c. results on pyrite (100 to 800 K) with literature values from precision adiabatic calorimetry." The Journal of Chemical Thermodynamics **11**(6): 567-584.
- NIST (2005). NIST Standard Reference Database Number 69.
- Nugene, T., Zavarin, E. and Barrall, E. M. (2003). "Effect of various parameters in differential scanning calorimetry of hydrogen-peroxide-treated lignocellulose." Journal of Applied Polymer Science **27**(3): 1019-1032.
- O'neil, M. J. (1966). "Measurement of specific heat functions by differential scanning calorimetry." Analytical Chemistry **38**(10): 1331-.
- Price, D. M. (1995). "Temperature calibration of differential scanning calorimeters." Journal of Thermal Analysis **45**: 1285-1296.

- Privalov, P. L. and Potekhin, S. A. (1986). "Scanning microcalorimetry in studying temperature-induced changes in proteins." Methods Enzymol **131**: 4-51.
- Ramakumar, K. L., Saxena, M. K. and Deb, S. B. (2001). "Experimental evaluation of procedures for heat capacity measurement by differential scanning calorimetry." Journal of Thermal Analysis and Calorimetry **66**: 387-397.
- Sarge, S. M., Gmelin, E., Höhne, G. W. H., Cammenga, H. K., Hemminger, W. and Eysel, W. (1994). "The caloric calibration of scanning calorimeters." Thermochimica Acta **247**: 129-168.
- Sarge, S. M., Hemminger, W., Gmelin, E., Hohne, G. W. H., Cammenga, H. K. and Eysel, W. (1997). "Metrologically based procedures for the temperature, heat and heat flow rate calibration of DSC." Journal of Thermal Analysis **49**: 1125-1134.
- Sarge, S. M., Höhne, G. W. H., Cammenga, H. K., Eysel, W. and Gmelin, E. (2000). "Temperature, heat and heat flow rate calibration of scanning calorimeters in the cooling mode." Thermochimica Acta **361**: 1-20.
- Sarri, H., Seo, D. Y., Blumm, J. and Beddoes, J. (2003). "Thermophysical property determination of high temperature alloys by thermal analysis." Journal of Thermal Analysis and Calorimetry **73**: 381-388.
- Schawe, J. E. K. (1993). "A new method to estimate transition temperatures and heats by peak form analysis." Thermochimica Acta **229**: 69-84.
- Schubnell, M. (2000). "Temperature and heat flow calibration of a DSC-instrument in the temperature range between -100 and 160 deg.C." Journal of Thermal Analysis and Calorimetry **61**: 91-98.

- Skoglund, P. and Fransson, A. (1996). "Accurate temperature calibration of differential scanning calorimeters." Thermochimica Acta **276**: 27-39.
- Speyer, R. F. (1994). Thermal Analysis of materials. New York, Marcel Dekker.
- Sturtevant, J. M. (1987). "Biochemical applications of differential scanning calorimetry." Annual Reviews Phys.Chem. **38**: 463-488.
- Trunov, M. A., Umbrajka, S. M., Schoenitz, M., Mang, J. T. and Dreizin, E. L. (2006). "Oxidization and melting of aluminum nanopowders." J. Phys. Chem. B **110**: 13094-13099.
- Van Wylen, G. J. and Sonntag, R. E. (1986). Fundamentals of classical thermodynamics, Wiley.
- Wang, D. and Overfelt, R. A. (2003). Differential scanning calorimetry measurements on molten magnesium alloys. Thermal Conductivity 27/Thermal expansion 15, DEStech Publications: 461-469.
- Wang, D., Overfelt, R. A. and Fasoyinu, Y. (2002). Thermophysical property measurements of a magnesium alloy, AE42. 131th TMS Annual Meeting, Seattle, WA.
- Wendlandt, W. W. (1986). Thermal Analysis. New York, Wiley.
- Wolfinger, M. G., Rath, J., Krammer, G., Barontini, F. and Cozzani, V. (2001). "Influence of the emissivity of the sample on differential scanning calorimetry measurements." Thermochimica Acta **372**: 11-18.
- Wu, R. I. and Perepezko, J. H. (2000). "Liquidus temperature determination in multicomponent alloys by thermal analysis." Metallurgical and Materials Transactions A **31A**: 497-501.